Solar Arrays for Low-Irradiance Low-Temperature and High-Radiation Environments

Base Period Final Report, Non-Proprietary Version
April 26th, 2017

NASA Extreme Environments Solar Power
Jet Propulsion Laboratory

PI: Andreea Boca, JPL
Co-I's: Paul Stella, JPL; Christopher Kerestes and Paul Sharps, SolAero

Introduction and background

This is the Base Period final report DRAFT for the JPL task "Solar Arrays for Low-Irradiance Low-Temperature and High-Radiation Environments", under Task Plan 77-16518 TA #21, for NASA's Extreme Environments Solar Power (EESP) project. This report covers the Base period of performance, 7/18/2016 through 5/2/2017.

The goal of this project is to develop an ultra-high efficiency lightweight scalable solar array technology for low irradiance, low temperature and high-radiation (LILT/Rad) environments. The benefit this technology will bring to flight systems is a >20% reduction in solar array surface area, and a six-fold reduction in solar array mass and volume. The EESP project objectives are summarized in the "NRA Goal" column of Table 1. Throughout this report, low irradiance low temperature (LILT) refers to 5AU -125°C test conditions; beginning of life (BOL) refers to the cell state prior to radiation exposure; and end of life (EOL) refers to the test article condition after exposure to a radiation dose of 4e15 1MeV e^-/cm^2.

Performance	NRA Goal
LILT BOL cell efficiency	35%
LILT EOL cell efficiency	28%
LILT EOL array specific power	8-10 W/kg
1AU BOL packaging density	60 kW/m^3
Stowed & launch capability	Yes
Operation in 100-300V range	Yes
Plasma operation 2eV, 1e8/cm^3	Yes
LILT EOL minimum array power	5 kW

Table 1. Summary of EESP project objectives.

The proposed solar array system technology combines two components: (1) advanced-architecture solar cells; and (2) lightweight scalable mechanical structures. The solar cell is a LILT and radiation-optimized version of SolAero's IMM4; the array structure is OATK's MegaFlex, a planar (i.e., non-concentrator) lightweight flexible blanket.

Fluence (e^-/cm^2)	Demonstrated	NRA Goal
0e00 (BOL)	37.9%	35.0%
4e15 (EOL)	29.5%	28.0%

Table 2. LILT (5AU -125°C) efficiency for the IMM4 cells upon conclusion of the Base period.

During the Base period, we evaluated two device architectures for the solar cell component: the inverted metamorphic four-junction cell (IMM4) as the primary concept; and the lattice-matched triple junction (ZTJ) as the back-up. For the array-structure component, we also considered two architectures: a planar large-scale lightweight blanket as the primary concept; and a concentrator system as the back-up. The cell design was iterated towards the goal of eliminating those features which limit performance under LILT and radiation conditions. The 0^{th} iteration consisted of baseline devices of 1AU-optimized design. The 1^{st} iteration was the first

step towards LILT optimization, and consisted of devices of modified design. The average LILT efficiencies demonstrated by test for the IMM4 cells of the 1st design iteration are summarized in Table 2; note that the demonstrated performance was found to meet both the LILT BOL and the LILT EOL cell efficiency targets.

A cell architecture trade study was completed upon conclusion of the 1st iteration, resulting in the downselect of the IMM4 over the ZTJ device structure. Also, an array-structure concept trade study was also completed at that time, resulting in the down-select of the planar over the concentrator architecture. Furthermore, a request for information (RFI) resulted in the selection of MegaFlex as the most suitable planar array-structure technology to go forward with for Options I and II. Preliminary analysis of the proposed solar array system, which combines the IMM4 cell and the MegaFlex structure, indicates that the technology is expected to meet the NRA goals as summarized in Table 1.

Technical description

Cell description

The device architecture that we have down-selected during the Base period is a modified version of SolAero's IMM4 solar cell, optimized for ultra-high performance in low irradiance, low temperature and high radiation (LILT/Rad) environments.

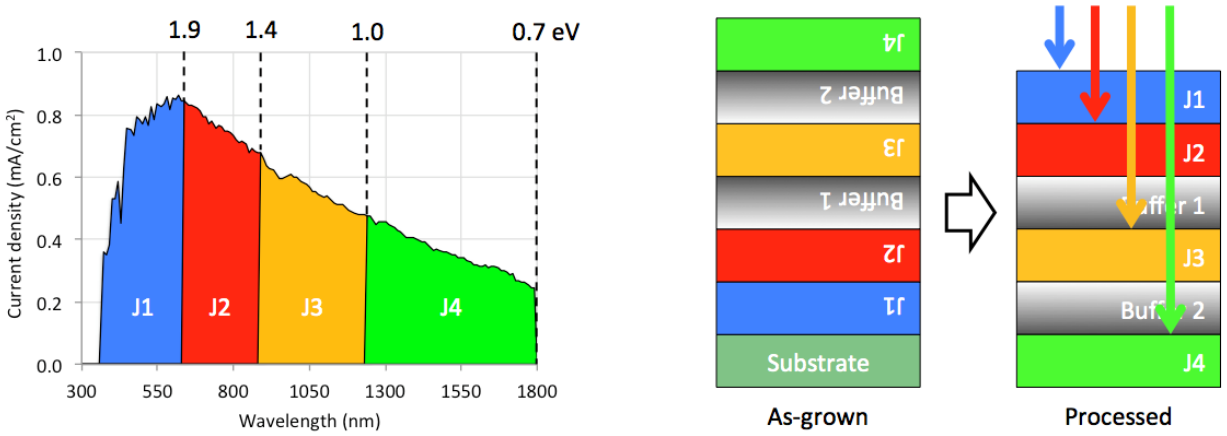

Figure 1. Schematic depiction of IMM4 design and fabrication.

As shown schematically in Figure 1, the IMM4 cell is a III-V inverted metamorphic four-junction device. The subcell bandgaps at room temperature are: J1 = 1.9eV, J2 = 1.4eV, J3 = 1.0eV and J4 = 0.7eV, which is the optimal bandgap combination for a four-junction device in the AM0 spectrum. Of the four subcells, J1 and J2 are lattice-matched to the growth substrate, whereas J3 and J4 are metamorphic. The MOCVD growth is inverted, meaning that J1 is grown first, followed by J2, then a first metamorphic graded buffer, followed by J3, then a second metamorphic graded buffer, then J4. During post-growth wafer processing, the cell is flipped over and attached to a 0.006"-thick glass carrier which is CTE-matched to the cell, then the growth substrate is removed. Both the n and the p metal contacts of the cell are accessible from the top (illuminated) side of the device. The LILT/Rad-optimized version of IMM4 has top contacts that have been optimized for operation at 5AU, which have already been implemented

during the 1st design iteration; as well as subcell current balancing that has been optimized for EOL (4e15 1MeV e-/cm^2) operation at -125°C, which is planned for implementation as part of the 2nd design iteration.

The first level of integration for an IMM4 solar cell is in a coverglassed interconnected cell (CIC) assembly, which consists of the following components: (1) IMM4 cell; (2) silicon bypass diode; (3) welded silver-clad Kovar interconnects; (4) DC93-500 optically transparent coverglass adhesive; and (5) 0.004"-thick CMG-AR coverglass. Aside from the solar cell, all other CIC and string components and materials are per the state-of-practice (SoP).

Array-structure description

The array-structure concept that we have down-selected during the Base period is a planar (i.e., non-concentrator) lightweight large-scale flexible blanket. Of the several currently available array-structure technologies that fall within this overall concept, through a recent RFI we found MegaFlex by Orbital ATK to be the most suitable for integration with the IMM4 cell technology, as well as for meeting the project's TRL timetable and performance objectives in the EESP environment.

MegaFlex has been recently developed to TRL-6 by NASA for 1AU solar electric propulsion (SEP) applications, and we expect that the same technology will be used for EESP without the need for significant further development at the structural level. The preliminary EESP design for a MegaFlex-based solar array producing >5kW at LILT EOL consists of two 17.8m-diameter wings.

Expected performance

The efficiency of the EESP cell component at the conclusion of development is expected to match or exceed the demonstrated performance as summarized in Table 2. The illuminated current-voltage (LIV) cell parameters as of the end of the Base period are summarized in Table 3. Power estimates based on the current-design IMM4 performance are conservative, since upcoming development during Option I is expected to result in additional performance improvements, through further design optimization for the LILT and radiation environment.

Dist. (AU)	Fluence (e-/cm^2)	Temp (C)	Voc (V)	Isc (A)	Vmp (V)	Imp (A)	Pmp (W)	Area (cm^2)
5	0e00	-125	4.076	0.0168	3.760	0.0152	0.0572	27.56
5	4e15	-125	3.826	0.0157	3.281	0.0135	0.0444	27.56

Table 3. LILT BOL and EOL LIV-curve parameters for IMM4, based on current performance.

Areal mass density at the CIC level is summarized in Table 4. The mass of the array structure, for the EESP array comprised of two 17.8m wings, is 302.2kg.

In order to predict the array-level power performance, a preliminary layout has been designed. The layout assumes a 45-cell string length, and a 65.2cm^2 cell size which corresponds to one of the standard form factors provided by SolAero. This layout is conservative since the cell form factor is not optimized for packing factor. The design has a total quantity of 51300 cells for the two-wing array, and a total CIC mass of 304.4kg. Therefore, the total array mass including both the CICs and the structure is 606.6kg.

Material	Thickness
Cover glass	0.004"
DC93-500	0.002"
Semiconductor	0.001"
Substrate glass	0.006"

Component	Mass (kg/m^2)
Cover glass	0.258
DC93-500	0.055
Bypass diode	0.009
Interconnects	0.011
Semiconductor	0.133
Contact metal	0.060
Substrate glass	0.387
CIC Total	**0.91**

Table 4. IMM4 CIC layer stack-up and mass per unit of active area.

Power model	LILT BOL	LILT EOL
Pmp w/o losses (W)	6937	5391
Series resistance	98.1%	98.0%
Blocking diodes	99.6%	99.5%
Voltage mismatch	99.5%	99.5%
Current mismatch	99.5%	99.5%
Array Pmp (W)	**6706**	**5206**
NRA goal (W)	N/A	5000

Table 6. Power model results for the preliminary array design producing >5kW at LILT EOL.

A preliminary array-level power model has been created, based on the layout and on the current performance of the IMM4 CICs as detailed in Table 3. The string-level Voc for the preliminary design is 183V at LILT BOL, and 172V at LILT EOL, both of which are in the required 100-300V operating range. The power model results are summarized in Table 6. Note that the array-level LILT power at end of life is in excess of 5kW, which meets the EESP NRA goal for scalability.

Based on the above power analysis, the array-level LILT specific power is 11.1W/kg at BOL and 8.6W/kg at EOL. Note that the array system meets the EESP NRA goal for LILT EOL specific power, of 8-10 W/kg.

The total 1AU BOL power for the array is estimated to be 138.1kW. Also, the actual stowed volume (as opposed to the larger envelope shown in Figure 2) is 2.58m^3 for the two wings. Therefore, the 1AU BOL packaging density is estimated to be 53.5 kW/m3, which falls short of the NRA goal of 60 kW/m3. The array technology could in principle be modified in order to

meet the as-stated packaging density requirement, e.g. by improving the 1AU BOL cell efficiency at the expense of its LILT EOL efficiency. However, array sizing for the intended EESP application is likely to be driven by LILT EOL performance rather than by 1AU BOL performance, since the incident solar resource available near 1AU is a factor of 25 higher than at 5AU. We would therefore recommend rewriting the packaging density requirement from the point of view of the intended LILT EOL capability of the array. For the proposed system, the LILT EOL packaging density is 2.02 kW/m^3.

The system performance is also expected to meet the NRA goals in terms of stowed and launch capability. For more information, please see the supporting data in the TRL assessment section of this report. As for operation in the 100-300V range in a plasma environment, we plan to verify this requirement by test during Option I; until then, our expectations for the system's performance are based on the favorable ESD results obtained on MegaFlex coupons under 1AU test conditions. More information on the supporting data can be found also in the TRL assessment section of this report.

Performance	Expected	NRA Goal
LILT BOL cell efficiency	37.9%	35%
LILT EOL cell efficiency	29.5%	28%
LILT EOL array specific power	8.6 W/kg	8-10 W/kg
1AU BOL packaging density	53.5 kW/m^3	60 kW/m^3
Stowed & launch capability	Yes	Yes
Operation in 100-300V range	Yes	Yes
Plasma operation 2eV, 1e8/cm^3	Yes	Yes
LILT EOL minimum array power	5.2 kW	5 kW

Table 7. Summary of expected system performance compared to the EESP project objectives.

Table 7 summarizes the results presented in this section on the expected performance of the array system, as compared to the EESP NRA goals.

Base period results

Background on the 0th iteration

As part of a previous JPL project (a FY16 R&TD task, distinct from EESP), a quantity of 12 IMM4 coverglassed interconnected cells (CICs) of baseline 1AU-optimized design were fabricated by SolAero. The active area was 27.56cm^2 for each CIC, and the coverglass was 0.004"-thick AR-coated CMG. Six of the twelve CICs were kept as unirradiated controls, and the other six were irradiated to a dose of 1e15 1MeV e$^-$/cm^2. The irradiation was performed in JPL's Dynamitron, at a flux rate of 1e10e$^-$/cm^2-s and at a sample temperature of -140°C. All CICs were tested in JPL's X25 LILT lab, under a simulated AM0 solar spectrum at 1AU +28°C, as well as at 5.5AU between -140°C and +28°C, both pre- and post-radiation. Once this work was completed, the previous project had no further use for the 12 IMM4 samples, and they were transferred to the EESP project where they were treated as the 0th cell design iteration.

On the EESP project, all 12 0th iteration CICs were X25 tested at 5AU -125°C to +28°C, at both 1× and 10× concentrations. Note that the irradiance for a 10× concentration at a 5AU sun distance corresponds to a 1× concentration at a 1.58AU sun distance, so for simplicity the 5AU 10× data throughout this report is labeled as "1.58AU". The six irradiated CICs received an additional dose of 3e15 1MeV e^-/cm^2, bringing the total accumulated dose to 4e15e^-/cm^2, which constitutes EOL per the EESP project requirements. The irradiation was performed once again in JPL's Dynamitron, at a flux rate of 1e10e^-/cm^2-s, and at a sample temperature of -125°C. All 12 CICs were re-tested at EOL in JPL's X25 lab. They were also visually inspected both before and after irradiation, to verify the integrity of the transparent adhesive (DC93-500) bond between the coverglass and the cell. In addition, for the purposes of checking the X25 test accuracy, the 28°C 1AU and 5AU tests were repeated in SolAero's SS08 4-zone solar simulator.

Test results from the 0th iteration

Figures 6 and 7 summarize the X25 results on 0th-iteration IMM4, as measured upon the project's receipt of the 12 CIC samples, at 5AU and 1.58AU respectively. The unirradiated controls are shown in blue, and the irradiated test cells in red; the test datapoints are plotted as markers, with the solid lines being polynomial fits that aid the eye by showing general trends in the average data. At this initial point in the EESP test sequence, the control samples had received no irradiation, whereas the test cells had been exposed to a 1e15 1MeV e^-/cm^2 dose. The plots show the temperature dependence of the most relevant illuminated current-voltage (LIV) curve parameters: open circuit voltage Voc; short circuit current density Jsc; fill factor (FF); and efficiency (Eff).

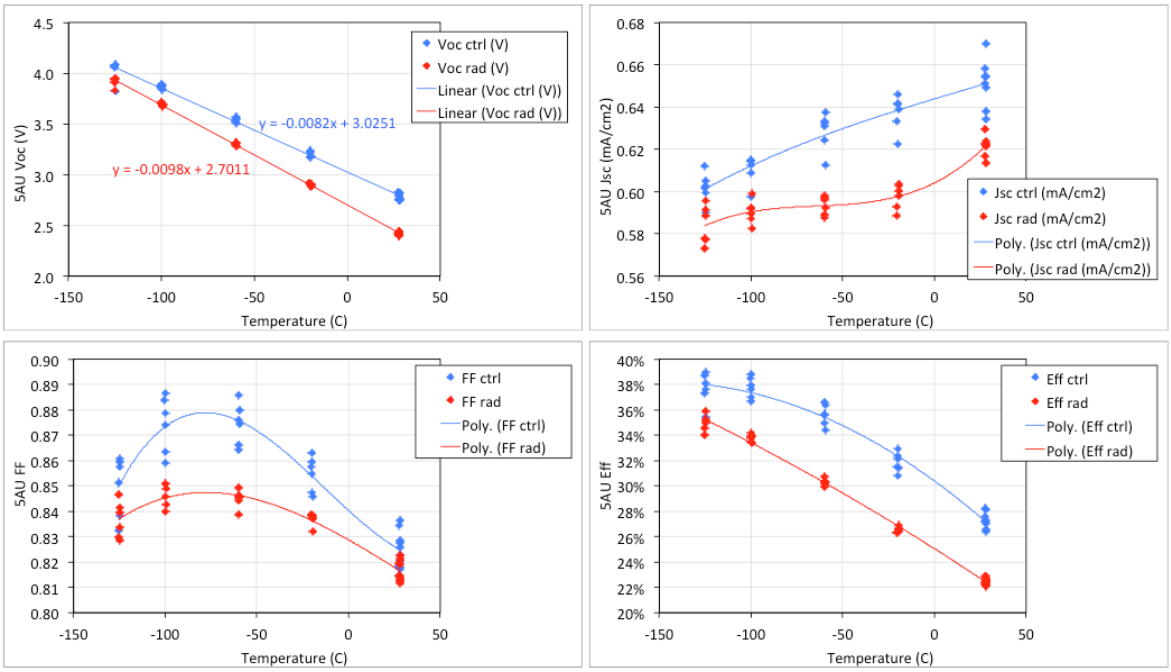

Figure 6. As-measured X25 LIV curve parameters at 5AU (1×), on 0th iteration IMM4 unirradiated controls (blue), and test cells irradiated to 1e15 1MeV e^-/cm^2 (red).

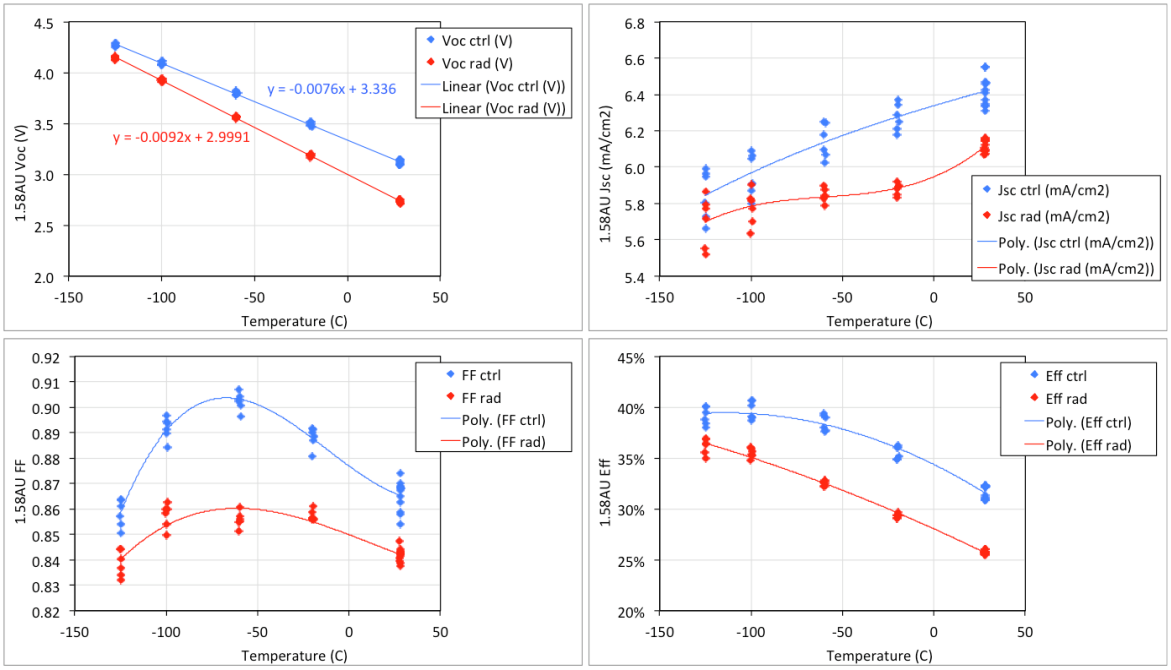

Figure 7. As-measured X25 LIV curve parameters at 1.58AU (10×), on 0th iteration IMM4 unirradiated controls (blue), and test cells irradiated to 1e15 1MeV e^-/cm^2 (red).

Visual inspection of all 12 0th-iteration IMM4 CICs yielded no indications of delamination or other damage, either before or after applying the additional dose of 3e15e^-/cm^2 to the six irradiated test cells. Figure 8 shows the six irradiated test cells at EOL after removal from the Dynamitron accelerator chamber, still tape-mounted on a thermal control plate.

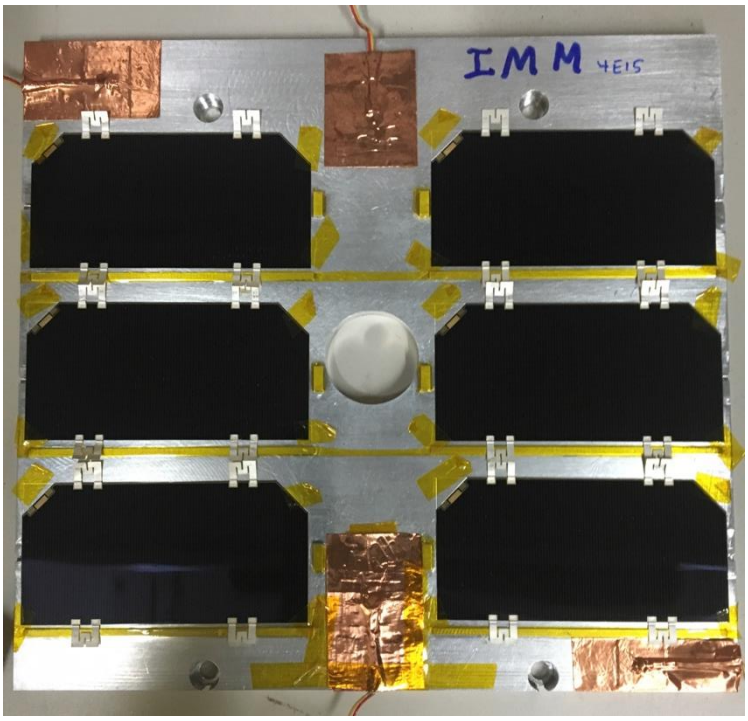

Figure 8. Irradiated 0th-iteration IMM4 CICs after EOL removal from the Dynamitron.

Figures 9 and 10 summarize the X25 results on 0th-iteration IMM4, as measured once the test cells had reached the EOL radiation dose, at 5AU and 1.58AU respectively. At this point in the test sequence, the control samples had still received no irradiation, whereas the test cells had been exposed to an accumulated 4e15 1MeV e^-/cm^2 fluence. The plotting conventions are analogous to those for Figures 2 and 3.

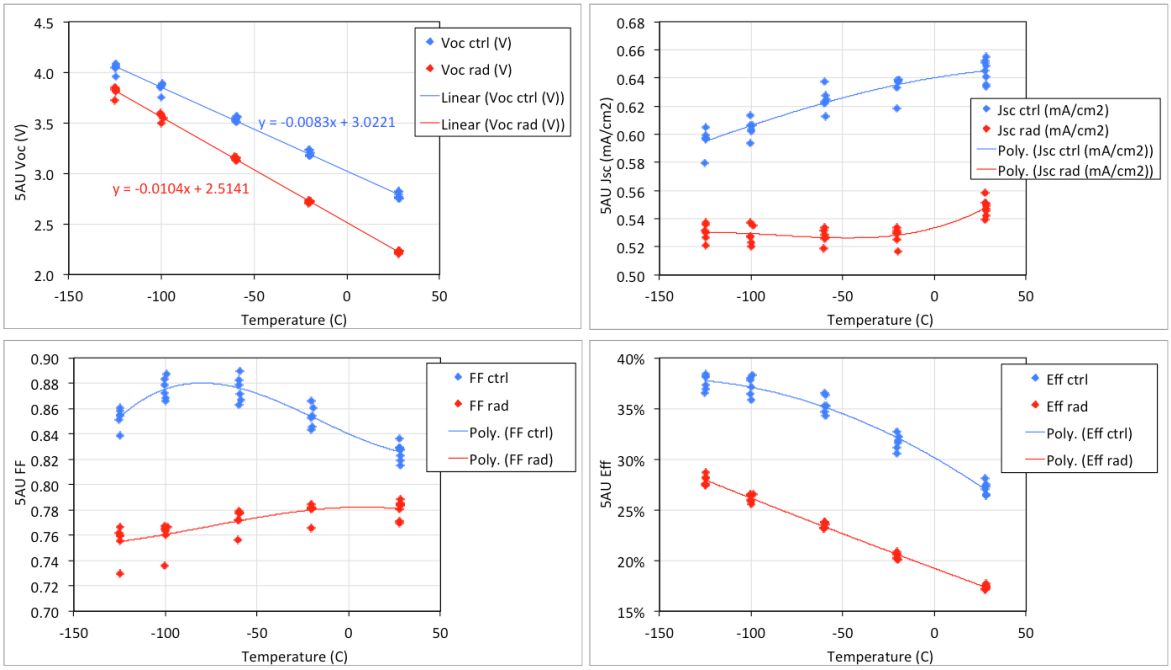

Figure 9. As-measured X25 LIV curve parameters at 5AU (1×), on 0th iteration IMM4 unirradiated controls (blue), and test cells irradiated to 4e15 1MeV e^-/cm^2 (red).

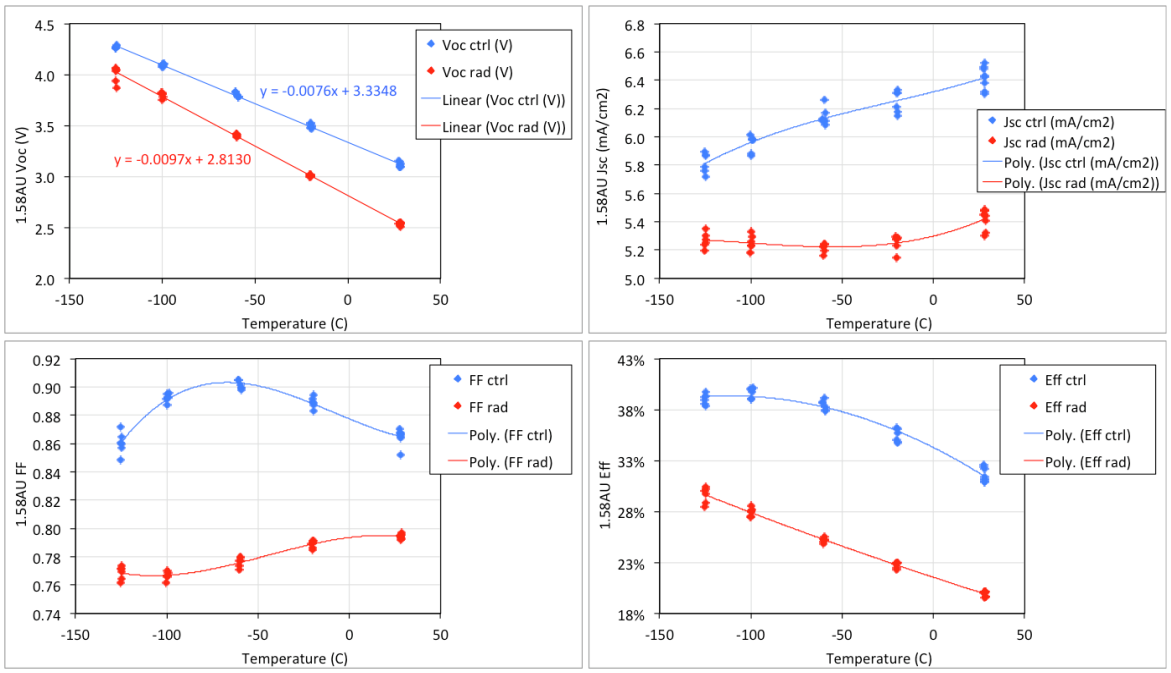

Figure 10. As-measured X25 LIV curve parameters at 1.58AU (10×), on 0th iteration IMM4 unirradiated controls (blue), and test cells irradiated to 4e15 1MeV e^-/cm^2 (red).

An overall observation that applies to the data shown in Figures 2 through 6 is that the Voc dependence on temperature is closely approximated by a straight line, which attests to the good thermal control of the CICs in the X25 test fixture.

Figure 11 shows example LILT LIV curves at -125°C. As before, the unirradiated controls are plotted in blue whereas the irradiated test cells are plotted in red. The change in the LIV curve shape with irradiation is primarily a softening of the shoulder, which can be explained by an increase in the effective ideality factor. However, radiation does not appear to significantly change the shunt resistance of the cells.

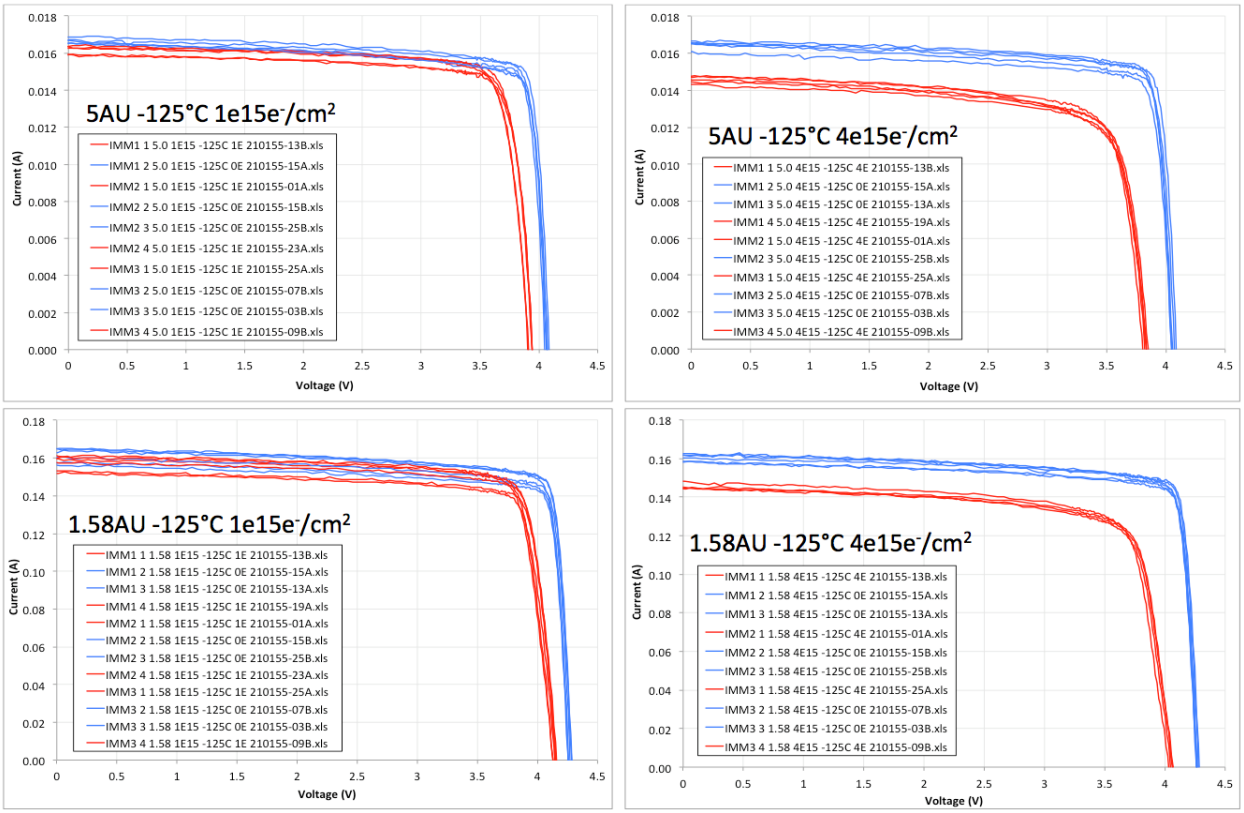

Figure 11. Example 0th iteration IMM4 LILT X25 LIV curves at -125°C, 5AU and 1.58AU. Unirradiated control cell data is in blue; irradiated test cell data is in red.

The 0th iteration IMM4 performance data at -125°C and +28°C is compiled in Figure 12, which shows the as-measured efficiency values in panel (a), and the remaining power fractions in panel (b). The same as-measured efficiency data is also listed in Table 8. The error bars represent one standard deviation over the measured data for the sample population of 6 control CICs at BOL (0e00 e^-/cm^2) and 6 test CICs at the two different radiation doses (1e15 and 4e15 1MeV e^-/cm^2). We note that the remaining power fraction after irradiation is significantly higher at -125°C than at +28°C. For example: at 5AU, $P/P_0 \approx 0.74$ at -125°C, versus $P/P_0 \approx 0.64$ at +28°C. This type of behavior is particular to IMM4 and has not been observed in other cell types such as ZTJ; for a detailed side-by-side comparison of IMM4 and ZTJ, please see the below subsection "Test results from the 1st iteration".

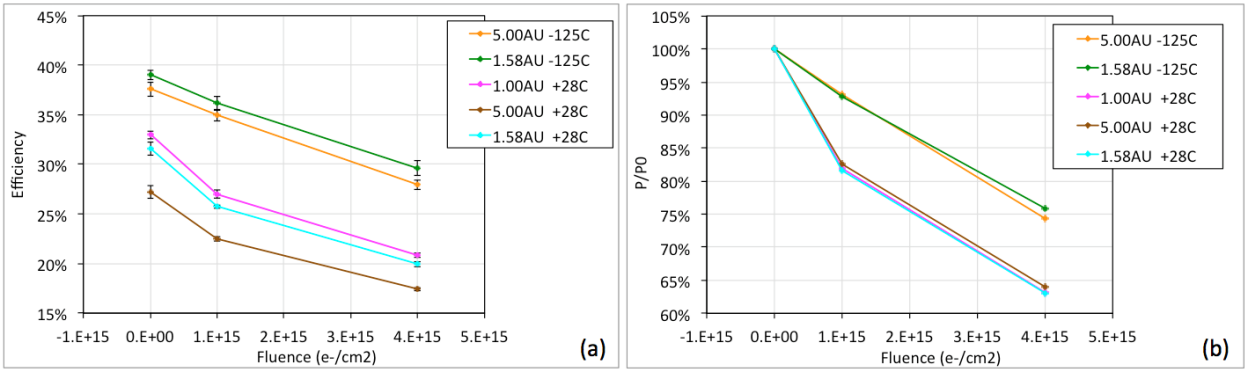

Figure 12. As-measured X25 data on IMM4 0th-iteration CICs at +28°C and -125°C, as a function of radiation fluence: (a) efficiencies; (b) remaining power fraction.

Fluence (e^-/cm^2)	Efficiency 5AU -125°C	Efficiency 1.58AU -125°C	Efficiency 1AU 28°C
0e00 (Ctrl)	37.6% ± 0.7%	39.0% ± 0.5%	33.0% ± 0.4%
1e15 (Rad)	35.0% ± 0.6%	36.2% ± 0.7%	27.0% ± 0.4%
4e15 (Rad)	27.9% ± 0.4%	29.6% ± 0.7%	20.8% ± 0.2%

Table 8. As-measured X25 efficiency data on 0th iteration IMM4, also plotted in Figure 12(a).

The unirradiated controls that were tested alongside the irradiated test cells were also used to quantify the precision of the X25 LILT test on IMM4. Figure 13 shows the efficiency dependence on temperature for the controls, at 5AU in panel (a) and at 1.58AU in panel (b). The markers designate as-measured data, whereas the lines are polynomial fits. The plot compares the data taken under nominally identical test conditions for the controls, at two different instances in the test sequence: first when the irradiated test cells were at the initial dose of 1e15e^-/cm^2, as designated by the empty markers and dashed lines; and second when the test cells were at 4e15e^-/cm^2, as designated by the filled markers and solid lines. Table 9 also summarizes the most relevant efficiency values measured on the controls at the same two test instances. The excellent agreement between the two test instances attests to the good reproducibility of the X25 test setup and procedure.

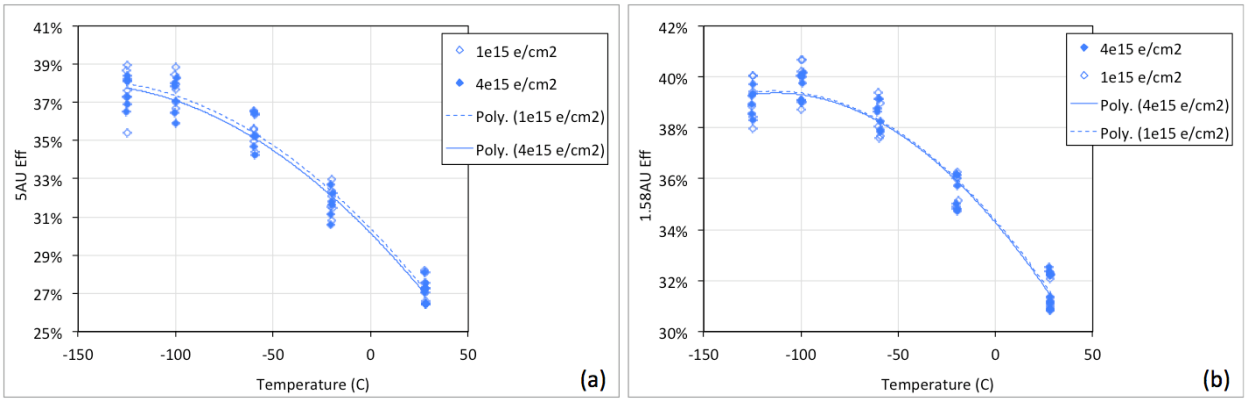

Figure 13. As-measured X25 efficiency test data on unirradiated controls tested alongside test cells that had been irradiated to 1e15 and 4e15e^-/cm^2, at (a) 5AU; and (b) 1.58AU.

Test cells fluence (e^-/cm^2)	Controls fluence (e^-/cm^2)	Controls eff. 5AU -125°C	Controls eff. 1.58AU -125°C	Controls eff. 1AU 28°C
1e15	0e00	37.7% ± 1.2%	39.1% ± 0.8%	33.4% ± 0.7%
4e15	0e00	37.6% ± 0.7%	39.0% ± 0.5%	33.0% ± 0.4%

Table 9. Key as-measured X25 efficiency data on unirradiated controls for the 0th cell iteration.

All the 0th-iteration LILT data discussed so far in this report was taken using JPL's X25, which is a 2-zone solar simulator, therefore not ideally suited for measuring 4-junction devices such as IMM4. As a first estimate of the X25's test accuracy for IMM4 at LILT, we performed a round-robin 28°C data comparison on the 12 IMM4 0th-iteration CICs, between the X25 and SolAero's SS08 4-zone solar simulator, at 1AU and at 5AU. At that stage in the project, the SS08 setup did not yet have the capability for low-temperature measurements.

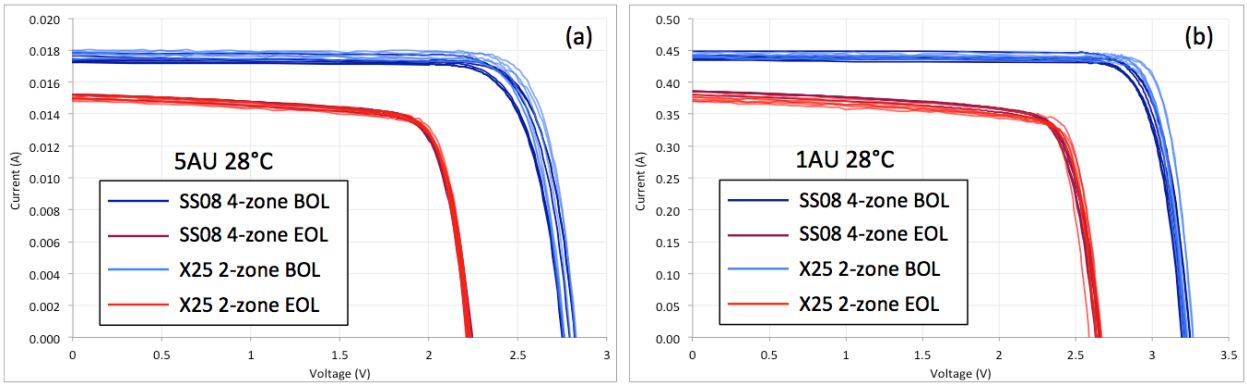

Figure 14. Comparison of 28°C LIV curves obtained on JPL's X25 2-zone versus SolAero's SS08 4-zone solar simulators, at (a) 5AU; and (b) 1AU.

Fluence (e^-/cm^2)	Voc	Isc	FF	Eff
0e00 (BOL)	100.2% ± 0.1%	102.0% ± 0.6%	102.1% ± 0.4%	104.4% ± 0.8%
4e15 (EOL)	99.8% ± 0.1%	99.3% ± 0.5%	101.8% ± 0.3%	100.8% ± 0.7%

Table 10. X25 (2-zone simulator) to SS08 (4-zone simulator) LIV parameter ratios for the 0th-iteration IMM4 data sets at 5AU 28°C.

Figure 14 shows the LIV curves on the control cells (blue) and on the EOL-irradiated test cells (red). The X25 2-zone data is plotted in lighter color shades, whereas the SS08 4-zone data is shown in darker shades. The average and standard deviation ratios of the most relevant LIV-curve parameters are shown in Table 10. In terms of measured efficiency, the BOL (control) measurement on the X25 was ~4% (relative) inflated with respect to the SS08; whereas the EOL (test cell) X25 measurement was only ~1% (relative) inflated. The X25 ÷ SS08 parameter ratios at 28°C were then used as correction factors on the LILT test data, the result of which is summarized in Table 11.

Upon conclusion of the 0th iteration milestone, without yet the performance benefit of any LILT design optimization, the IMM4 devices already come close to meeting the project objectives for cell efficiency at LILT BOL and EOL.

Fluence (e^-/cm^2)	As-measured	Corrected	NRA goal
0e00 (BOL)	37.6% ± 0.7%	36.0% ± 0.7%	35.0%
4e15 (EOL)	27.9% ± 0.4%	27.7% ± 0.4%	28.0%

Table 11. LILT (5AU -125°C) efficiency summary for the 0th-iteration IMM4 cells.

In parallel with the LILT LIV testing outlined above, we also performed external quantum efficiency (EQE) testing on IMM4, in JPL's recently developed low-temperature spectral response apparatus. Such tests enable us to determine the current balance between the four subcells as a function of temperature and irradiation dose, which informs the design optimization for subsequent development, starting with the 2nd iteration.

Background on the 1st Iteration

As part of the design process for the 1st-iteration cells, SolAero performed modeling of IMM4 and ZTJ using 0th-iteration and other prior data. The goal of the modeling was to optimize the front metal contact design for 5AU -125°C; and also, to optimize the antireflection coating (ARC) and epi-layer design for current balance at LILT EOL.

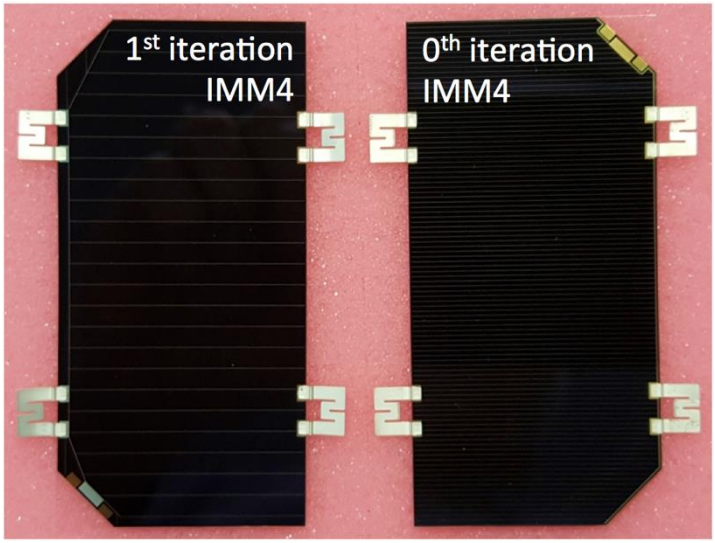

Figure 17. Grid design comparison between the 0th iteration IMM4 (right), optimized for 1AU 28°C; and the 1st iteration IMM4 (left), optimized for 5AU -125°C.

The primary conclusions that emerged from these models can be summarized as follows:

(1) Grid modeling showed that a LILT-optimized top contact design for ZTJ and IMM4 would result in ≥1.5% relative improvement over the 1AU-optimized baseline top contacts. The LILT-optimized grid design was therefore implemented for the 1st iteration.

(2) Epi-layer and ARC modeling for ZTJ showed that changes to optimize the cell design for current balance at EOL would result in negligible impact on performance. No epi-layer or ARC design changes were therefore pursued for ZTJ as part of the 1st iteration.

(3) High-fidelity epi-layer modeling of IMM4 would require low-temperature BOL and EOL external quantum efficiency (EQE) data, which was not yet available at that time.

Therefore, epi-layer changes in IMM4 will be implemented only with the 2nd iteration, allowing the design to be informed by the low-temperature EQE data.

(4) The ARC model for IMM4 suggested that a ~1.5% relative improvement can be obtained by optimizing for LILT; however, the model had large uncertainties. Therefore, as a risk-reduction strategy, an ARC split was implemented for the 1st iteration: samples were fabricated both with the process of record (PoR) unmodified ARC design, and with the modified design that had emerged from the modeling.

Following upon these design decisions, SolAero completed the growth, fabrication, CICing, 28°C (1AU and 5AU) 4-zone SS08 testing and delivery to JPL of 42 1st-iteration CICs, as follows: 14 ZTJ test articles with LILT-optimized grid design; 12 IMM4 test articles with LILT-optimized grids and PoR ARC; 8 IMM4 test articles with LILT-optimized grids and modified ARC; 4 IMM4 mechanical samples; and 4 ZTJ mechanical samples. The mechanical samples are 1AU electrical rejects which are however thermo-mechanically identical to the test articles. Same as for the 0th iteration, the active area for the 1st-iteration was 27.56cm^2 for each CIC, and the coverglass was 0.004"-thick AR-coated CMG. Two samples from the 0th and 1st cell iterations are shown side by side in Figure 17, which visually highlights the difference in top contact coverage (grid pitch and bus bar width).

All 1st iteration IMM4 CIC test articles, and 12 of the ZTJ test articles were X25 tested at BOL 5AU -125°C to +28°C, at both 1× and 10× concentrations; and also at 1AU +28°C. Based on the BOL data, the ARC design for IMM4 was down-selected to PoR, and the modified-ARC IMM4 samples were not tested any further. Six of the IMM4 PoR-ARC test articles, and six of the ZTJ test articles were irradiated to an EOL dose in the electron accelerator facility at NIST Gaithersburg, with the remaining six samples of each type being set aside as unirradiated controls. Then, all twelve samples of each of the two cell types were re-tested in the X25 at EOL 5AU -125°C to +28°C, at both 1× and 10× concentrations; and also at 1AU +28°C.

BOL test results from the 1st iteration

This section covers the pre-radiation test data obtained on the 1st-iteration CICs: IMM4 with PoR ARC, IMM4 with modified ARC, and ZTJ.

Figures 18 and 19 plot the LIV curve parameters as a function of temperature, for the twelve 1st-iteration IMM4 CICs with PoR ARC, at 5AU (1×) and at 1.58AU (10×) respectively: open-circuit voltage Voc; fill factor FF; short-circuit current Isc; and efficiency Eff. As before, the test datapoints are plotted as markers, with the solid lines being polynomial fits that aid the eye by showing general trends in the average data. We once again note that the Voc dependence on temperature is closely approximated by a straight line, which attests to the good thermal control of the CICs in the X25 test fixture.

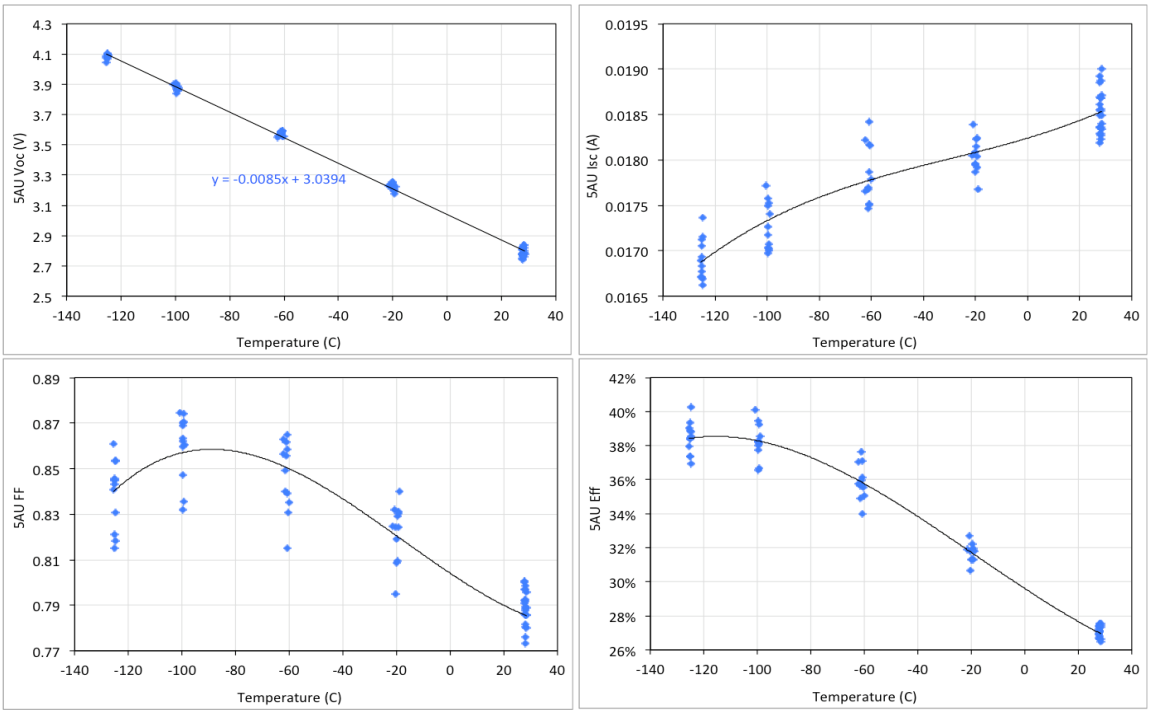

Figure 18. As-measured X25 LIV curve parameters at 5AU (1×), on the twelve 1st-iteration IMM4 unirradiated (BOL) CICs with LILT-optimized grids and PoR ARC.

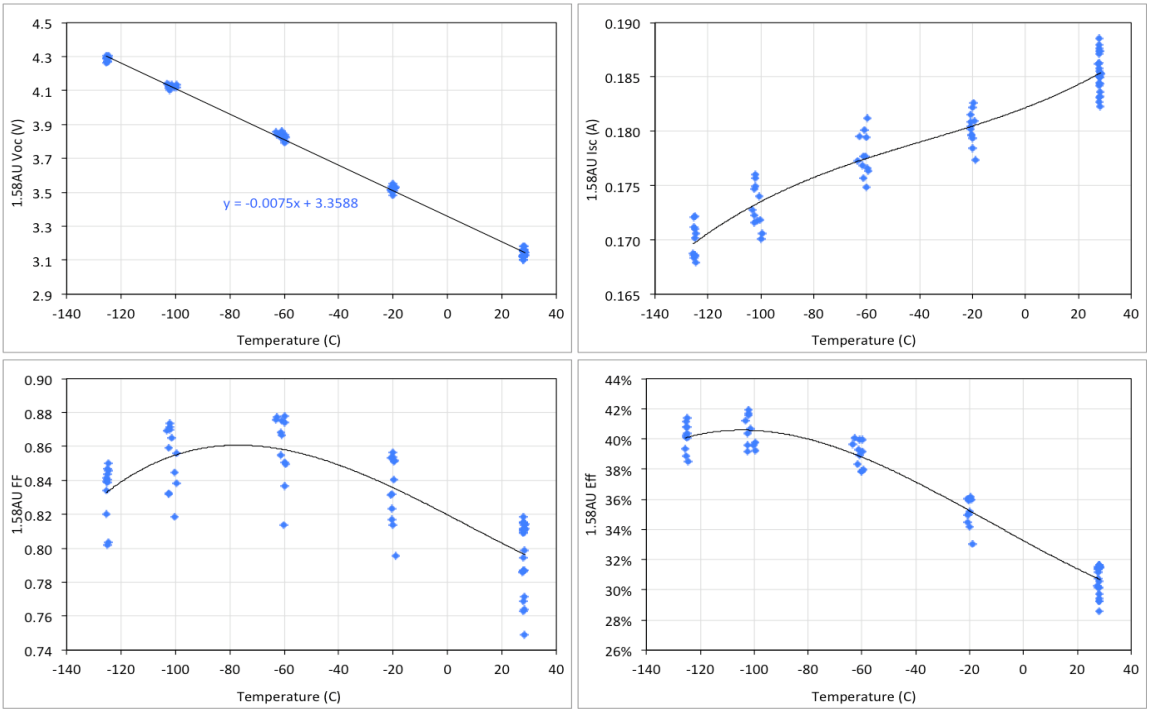

Figure 19. As-measured X25 LIV curve parameters at 1.58AU (10×), on the twelve 1st-iteration IMM4 unirradiated (BOL) CICs with LILT-optimized grids and PoR ARC.

LILT (5AU -125°C) LIV Parameter	Voc	Isc	FF	Eff
0th iteration (1AU 28°C grids)	4.061V	16.4mA	0.853	37.7%
1st iteration (5AU -125°C grids)	4.083V	16.9mA	0.839	38.4%
1st/0th parameter ratio	100.5%	103.0%	98.4%	101.9%

Table 12. LILT X25 LIV parameter comparison of 0th-iteration IMM4 BOL controls with 1AU-optimized grids, versus 1st-iteration IMM4 BOL CICs with LILT-optimized grids.

The only nominal difference between the 0th-iteration IMM4 control CICs, and the 1st iteration IMM4 CICs with PoR ARC, is in the top-contact grid design. Specifically, the grids are optimized for 1AU 28°C in the case of the 0th iteration, and for 5AU -125°C in the case of the 1st iteration. Therefore, the expectation based on SolAero's grid modeling is that, as compared to the 0th iteration, the 1st iteration would have the following features: (1) increased Isc due to reduced grid obscuration; (2) reduced FF due to increased series resistance; (3) slightly increased Voc due to a reduction in dark current; (4) overall increased efficiency by ~1.5% relative. The actual, as-measured LIV parameter comparison at LILT is summarized in Table 12, with example LIV curves at 5AU being shown in Figure 20. The measured performance improvement from the 0th to the 1st IMM4 iteration matches well with the model's qualitative predictions.

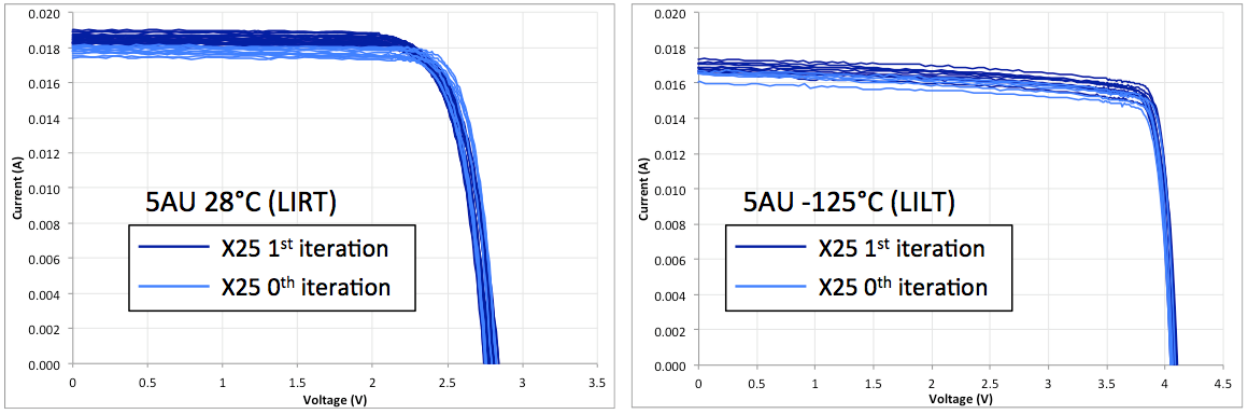

Figure 20. X25 LIV curves on 0th-iteration IMM4 controls with 1AU-optimized grids (light blue) and on 1st-iteration IMM4 CICs with LILT-optimized grids at BOL (dark blue).

Figures 21 and 22 show the illuminated current-voltage (LIV) performance of the eight IMM4 CICs with modified ARC, as-measured in the X25 LILT facility as a function of temperature, at 5AU and 1.58AU respectively.

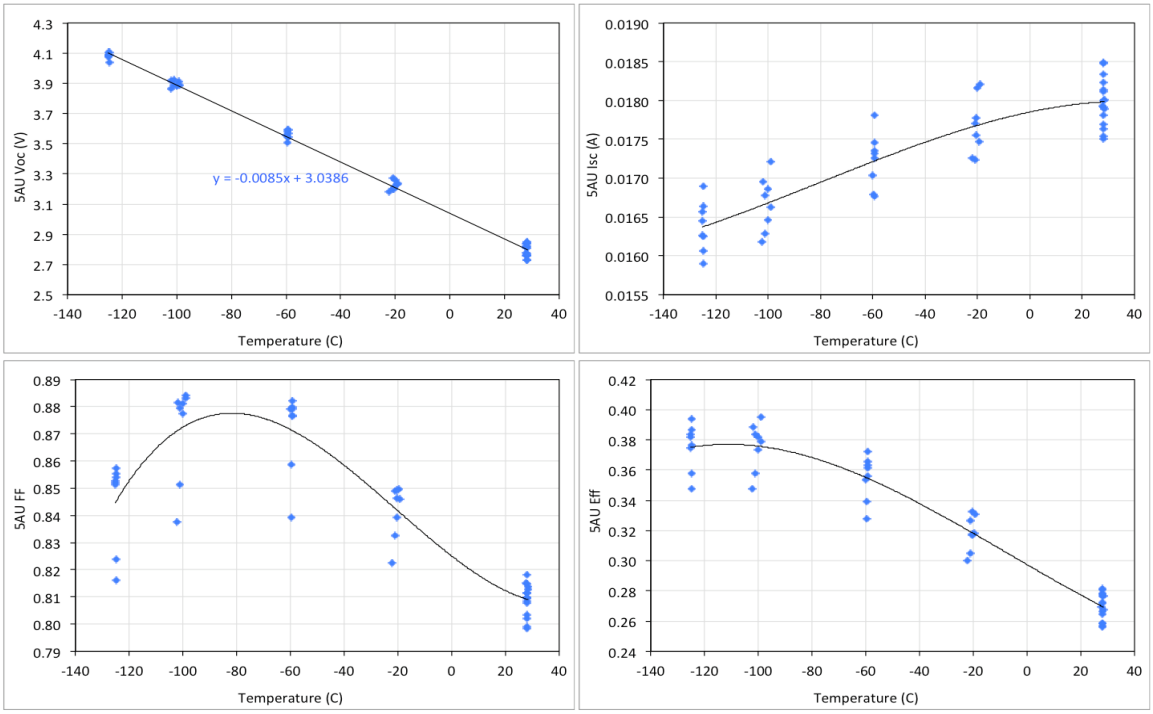

Figure 21. As-measured X25 LIV curve parameters at 5AU (1×), on eight 1st-iteration IMM4 unirradiated (BOL) CICs with LILT-optimized grids and modified ARC.

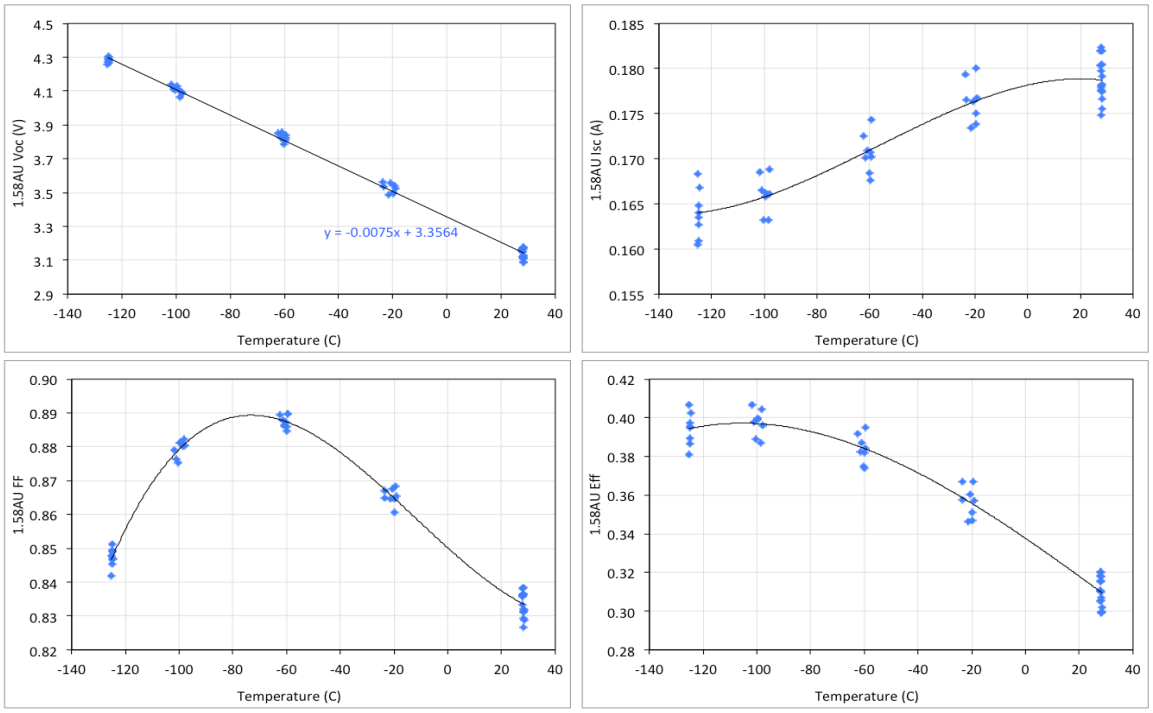

Figure 22. As-measured X25 LIV curve parameters at 1.58AU (10×), on eight 1st-iteration IMM4 unirradiated (BOL) CICs with LILT-optimized grids and modified ARC.

The most relevant as-measured average and standard deviation BOL efficiencies for the 1st-iteration IMM4 data set are summarized in Table 13. Based on this BOL data set, we downselected the IMM4 ARC design to PoR, and eliminated from consideration the modified

ARC, which had consistently shown slightly lower LILT performance than the PoR. From this point forward, when we refer to IMM4 we will mean only the PoR ARC version.

1st-iteration CIC Type	BOL Efficiency 5AU -125°C	BOL Efficiency 1.58AU -125°C
IMM4 - PoR ARC	38.4% ± 0.9%	40.1% ± 0.8%
IMM4 - Mod ARC	37.5% ± 1.4%	39.4% ± 0.8%

Table 13. As-measured X25 BOL average and standard deviation efficiency values for the two types of IMM4 1st-iteration CICs: twelve with PoR ARC and eight with modified ARC.

Figures 23 and 24 show the LILT LIV performance parameters for twelve of the 1st-iteration ZTJ CICs, as a function of temperature, at 5AU and at 1.58AU respectively.

The IMM4 and ZTJ sample populations, being comprised of 12 samples each, were divided into test and control populations of 6 samples each. The test populations were intended for EOL irradiation exposure, whereas the control populations were to be left unirradiated. Based on the BOL data set, we found that in all cases the average efficiency at 1AU and at LILT for the control population was within <0.1% absolute of the corresponding average efficiency for the test-cell population. In other words, for both IMM4 and for ZTJ, the cells designated as controls were found to be adequately representative of the test cells.

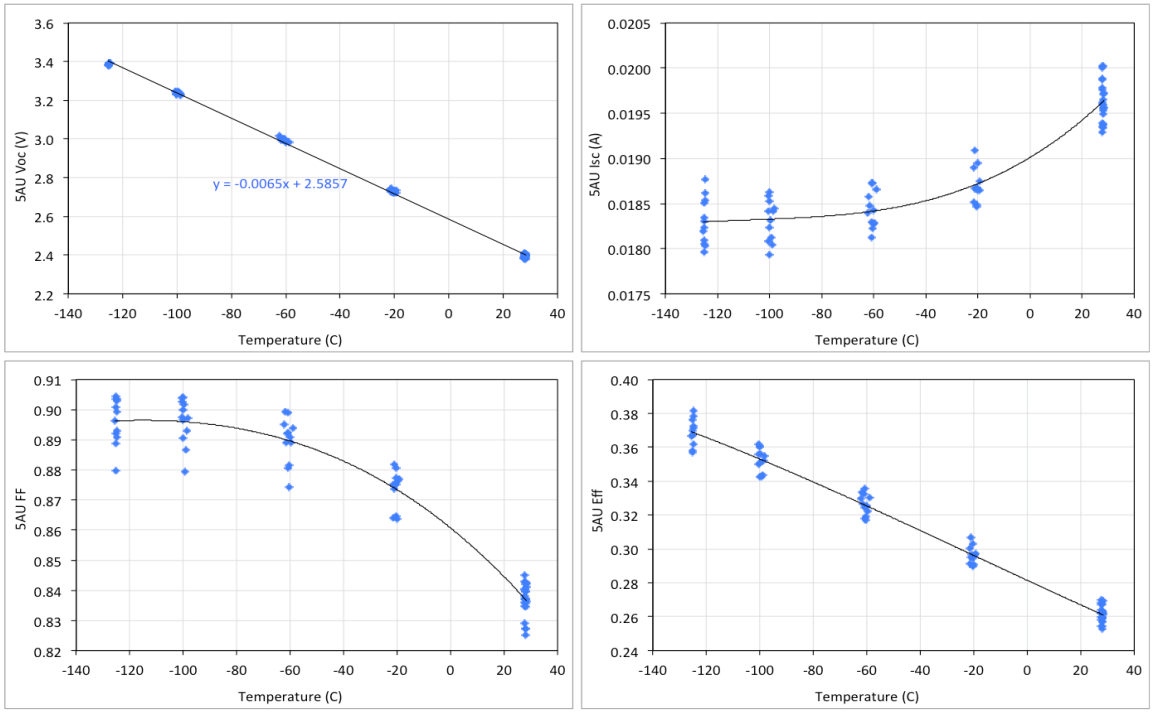

Figure 23. As-measured X25 LIV curve parameters at 5AU (1×), on twelve 1st-iteration ZTJ unirradiated (BOL) CICs with LILT-optimized grids.

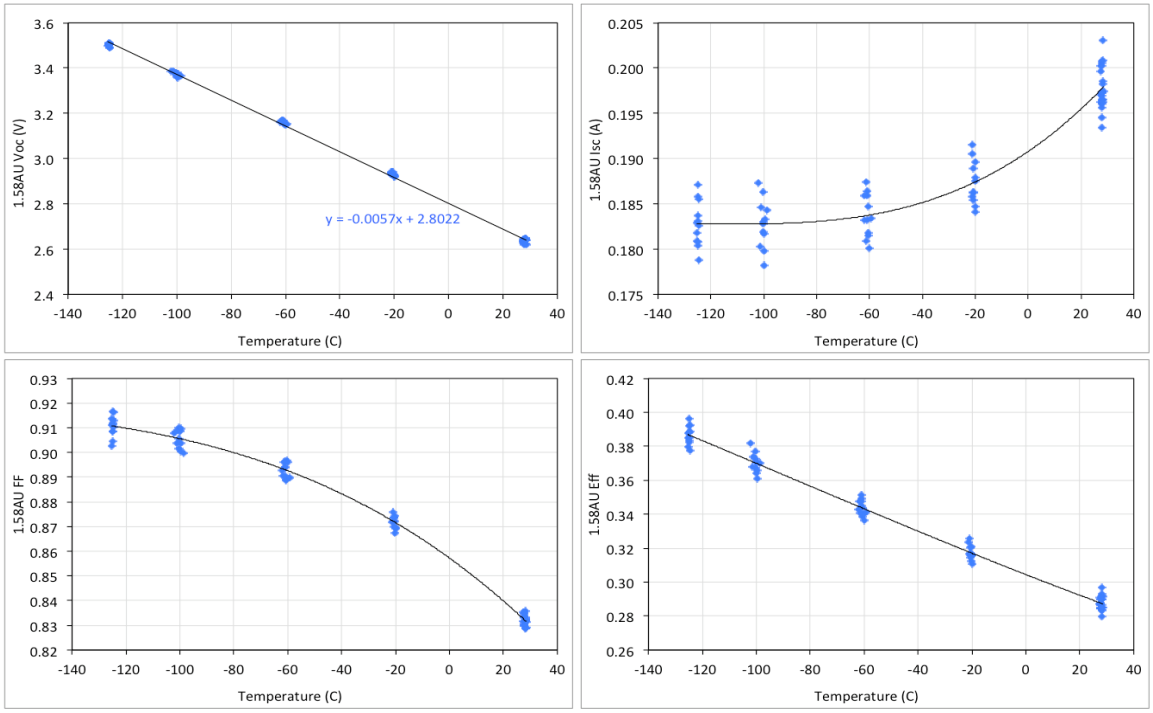

Figure 24. As-measured X25 LIV curve parameters at 1.58AU (10×), on twelve 1st-iteration ZTJ unirradiated (BOL) CICs with LILT-optimized grids.

Development of alternative radiation facility

The radiation exposure for the 1st iteration test articles had been originally planned to occur in the Dynamitron electron accelerator at JPL, same as for the 0th iteration. However, early in the EESP project it was found that the Dynamitron facility would require extensive maintenance during the Base period, causing long periods of down-time with significant uncertainties in their exact scheduling. We therefore set out to investigate the suitability of the NIST-Gaithersburg electron accelerator facility as an alternative to the Dynamitron.

One difference between the two facilities is that NIST only has the capability for room-temperature sample exposure, unlike the Dynamitron which can maintain the samples at low temperatures such as -125°C during irradiation. Note however that, regardless of their temperature during irradiation, in both cases the test articles would have to be stored for a time at room temperature just prior to the LILT test. In other words, neither the Dynamitron nor the NIST facility have the ability to perform LIV testing in situ, without first removing the samples from the accelerator chamber and bringing them to ambient conditions. By discussing these considerations with EESP project management, it was determined that maintaining low temperatures during irradiation was not a requirement, meaning that room temperature exposure would be just as suitable for the 1st cell iteration. The wisdom of this decision was later confirmed once the post-radiation 1st-iteration data was acquired and analyzed. Namely, given the design differences between them and as detailed below, the 0th and the 1st-iteration samples were expected to show similar average P/P_0 remaining power fractions after exposure to radiation; and the data indeed showed no significant difference between the two populations, despite the fact that the irradiation temperature had been -125°C for the 0th

iteration, and room temperature for the 1st. This confirmed our original assumption that the exact sample temperature during irradiation would not significantly affect the outcome.

Another key difference between the two facilities is that the NIST accelerator typically uses a higher flux rate of 4E11e$^-$/cm^2-s duty-cycle averaged, as compared to 1e10e$^-$/cm^2-s steady state for the Dynamitron. The higher flux rate introduces the risk of non-flight-like damage to the test articles, specifically delamination of the DC93-500 transparent adhesive between the coverglass and cell. Depending on its severity, such delamination can unfavorably skew the data in an overly conservative direction; in other words, the delamination artifacts would cause the ground-measured efficiencies to be significantly lower than they would be in flight. In order to minimize the risk of delamination in the test articles, we decided to use the mechanical CICs for a series of dry run experiments to determine the effect of the test-radiation-retest sequence on sample integrity.

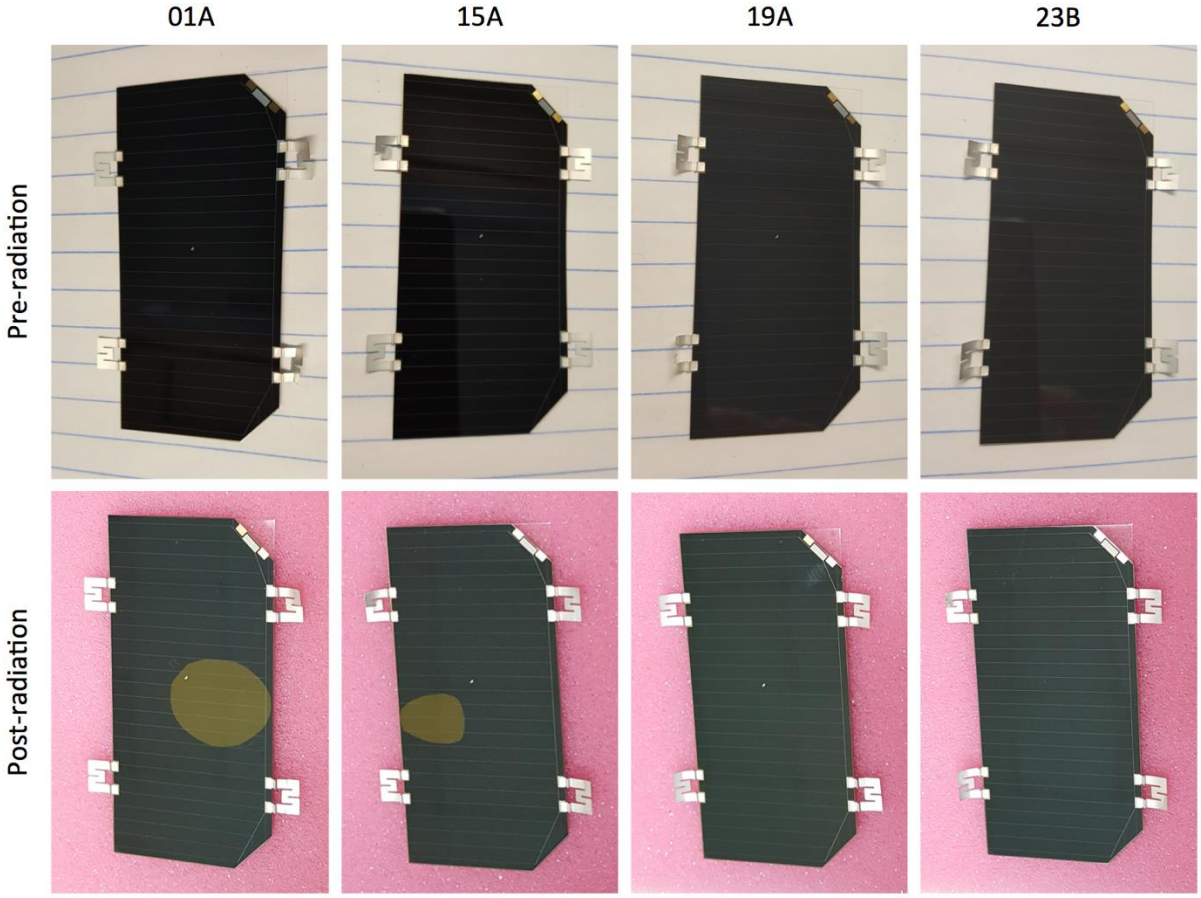

Figure 25. 1st-iteration IMM4 mechanical CICs before and after the first NIST irradiation dry run; note the radiation-induced DC93-500 delamination in samples 01A and 15A.

In a first dry run experiment, the four IMM4 mechanical samples were put through an X25 LILT test sequence at BOL, for the purpose of exposing them to the same thermal environment that the test articles would experience as part of their test sequence. Then, the mechanical samples were shipped to NIST where they were irradiated to an EOL dose at the standard flux rate of 4E11e$^-$/cm^2-s, duty-cycle averaged. Finally, they were put through an X25 LILT test sequence at EOL, once again for the purpose of simulating the thermal environment that the test articles

would experience. Before and after each test and exposure, the samples were visually inspected for signs of damage. Figure 25 shows photos of the four samples before shipping to NIST on the top row, and also after receiving them back at JPL post-radiation exposure on the bottom row. Note that the irradiation had caused two of the four samples (01A and 15A) to develop DC93-500 delamination, which appears in the photos as roughly circular gold-brown areas. This meant that the standard irradiation flux introduced a high likelihood of delamination, and that less aggressive flux conditions would need to be identified prior to using the NIST facility on the test articles.

In a second dry run experiment, the four ZTJ mechanical samples were put through the BOL X25 LILT thermal/test; they were then irradiated at NIST at an average flux rate of 8e10 e^-/cm^2-s, which is a 1/5× reduction with respect to the standard rate; and finally they went through the EOL X25 LILT test. This time, visual inspection of the samples found no sign of delamination or damage at any stage of the test-radiation-retest sequence. This indicated that we had successfully identified a radiation flux which poses only a low risk of delamination, and that the NIST facility would from now on be suitable for irradiating test articles.

EOL test results from the 1st iteration

The 1st-iteration test samples that had been designated for irradiation, i.e. 6 CICs each of IMM4 and ZTJ, were irradiated at NIST to an EOL dose of 4e15e^-/cm^2 using the reduced 8e10e^-/cm^2-s flux rate. Visual inspection of the irradiated test samples yielded no indications of delamination or other damage, before or after the radiation exposure. The test samples and the controls were then retested under nominally identical conditions as at BOL.

Figures 26 and 27 summarize the X25 results on 1st-iteration IMM4, as measured at 5AU and 1.58AU respectively. The unirradiated controls are shown in blue, and the irradiated test cells in red. The control samples were at BOL, having received no irradiation, whereas the test cells were at EOL, having been exposed to a 4e15 1MeV e^-/cm^2 EOL dose. Similarly, figures 28 and 29 summarize the X25 results on 1st-iteration ZTJ, at 5AU and 1.58AU respectively. The plotting conventions are analogous to those for Figures 21 and 22.

Figure 30 shows the LILT LIV curves at -125°C, for 1st-iteration IMM4 and ZTJ. As before, the unirradiated controls are plotted in blue whereas the irradiated test cells are plotted in red. For IMM4, the curves follow the same trends as for the 0th iteration: the change in the LIV curve shape with irradiation is primarily a softening of the shoulder, which can be ascribed to an increase in the effective ideality factor; however, radiation does not appear to significantly change the shunt resistance of the cells. By contrast, for ZTJ, radiation does cause a clear decrease in the shunt resistance, which impacts the fill factor and efficiency.

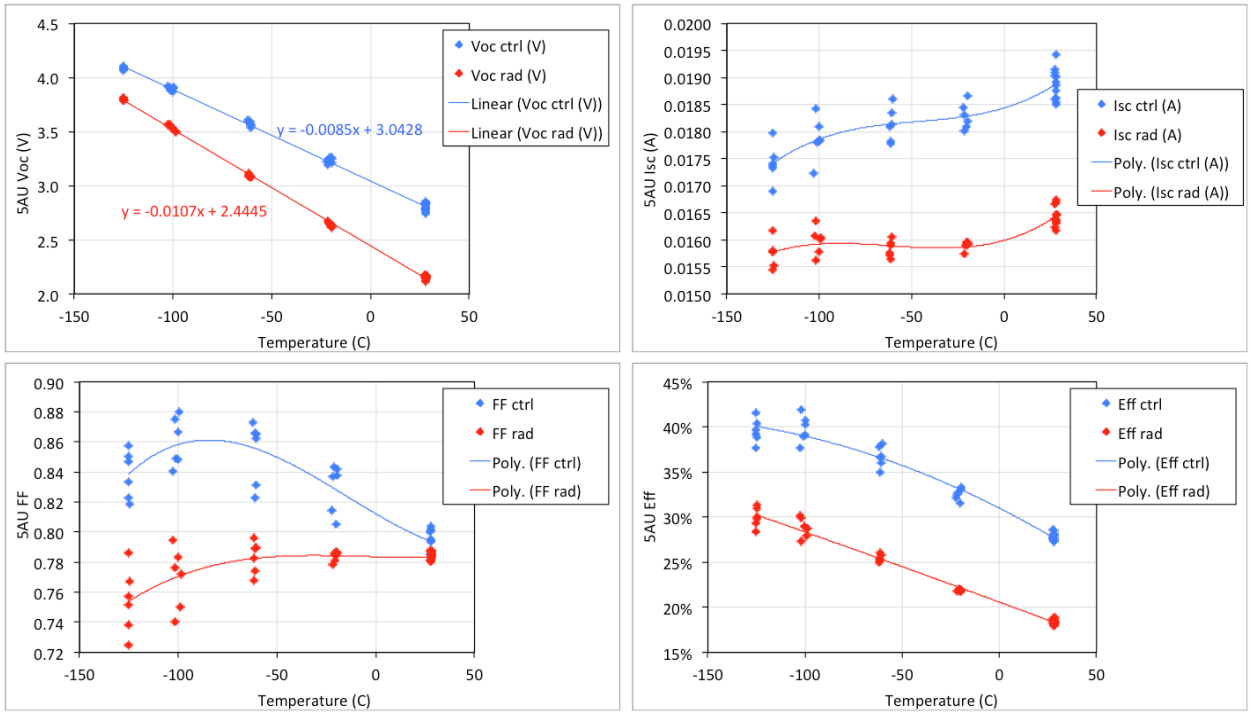

Figure 26. As-measured X25 LIV curve parameters at 5AU, on 1st iteration IMM4 unirradiated controls (blue), and test cells irradiated to 4e15 1MeV e^-/cm^2 (red).

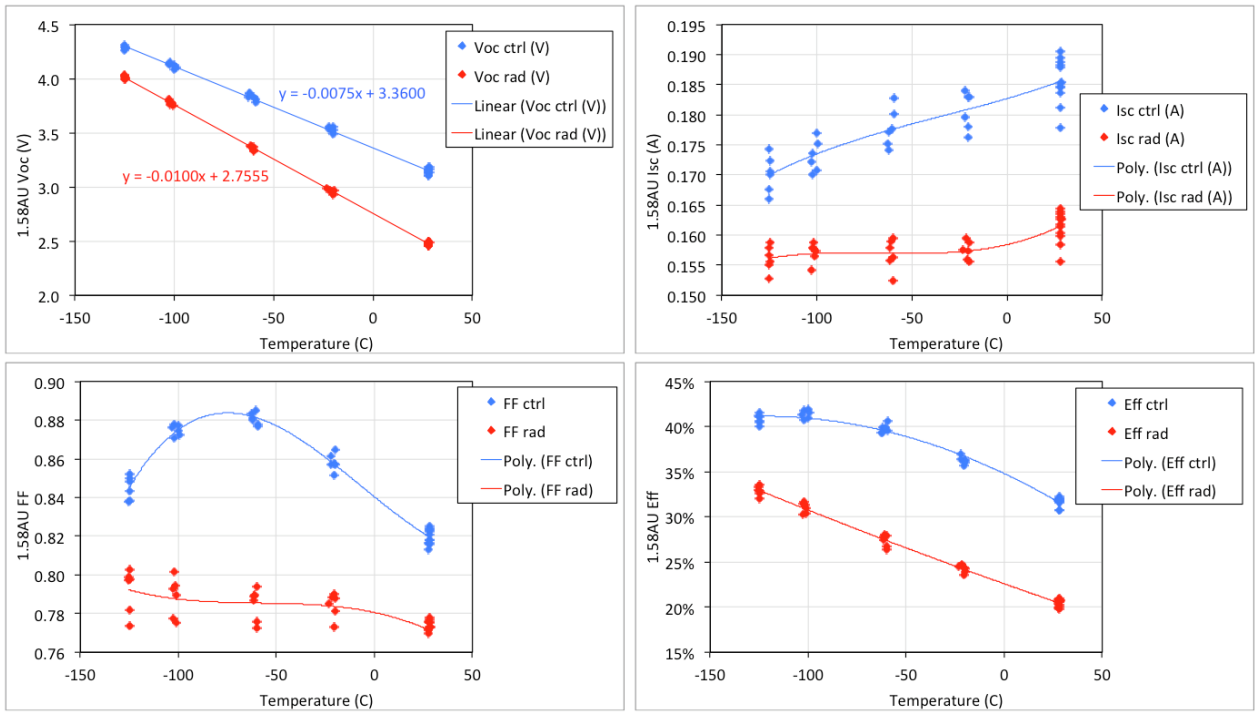

Figure 27. As-measured X25 LIV curve parameters at 1.58AU (10×), on 1st iteration IMM4 unirradiated controls (blue), and test cells irradiated to 4e15 1MeV e^-/cm^2 (red).

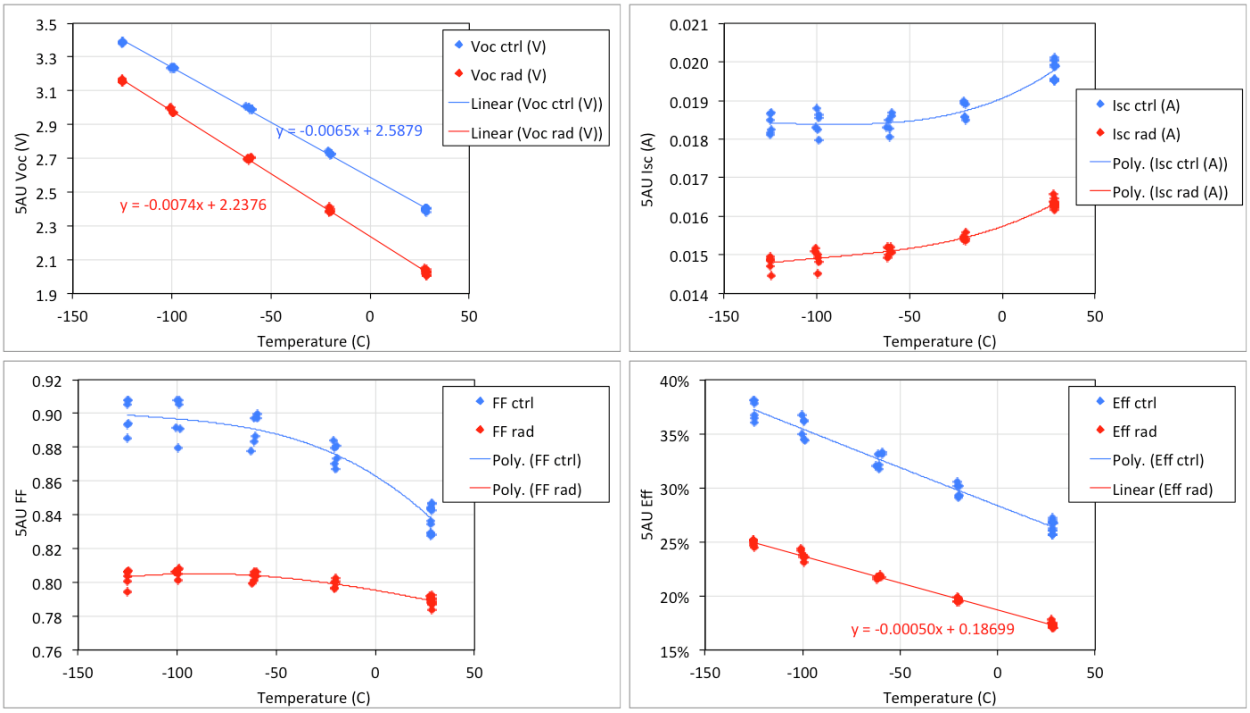

Figure 28. As-measured X25 LIV curve parameters at 5AU, on 1st iteration ZTJ unirradiated controls (blue), and test cells irradiated to 4e15 1MeV e^-/cm^2 (red).

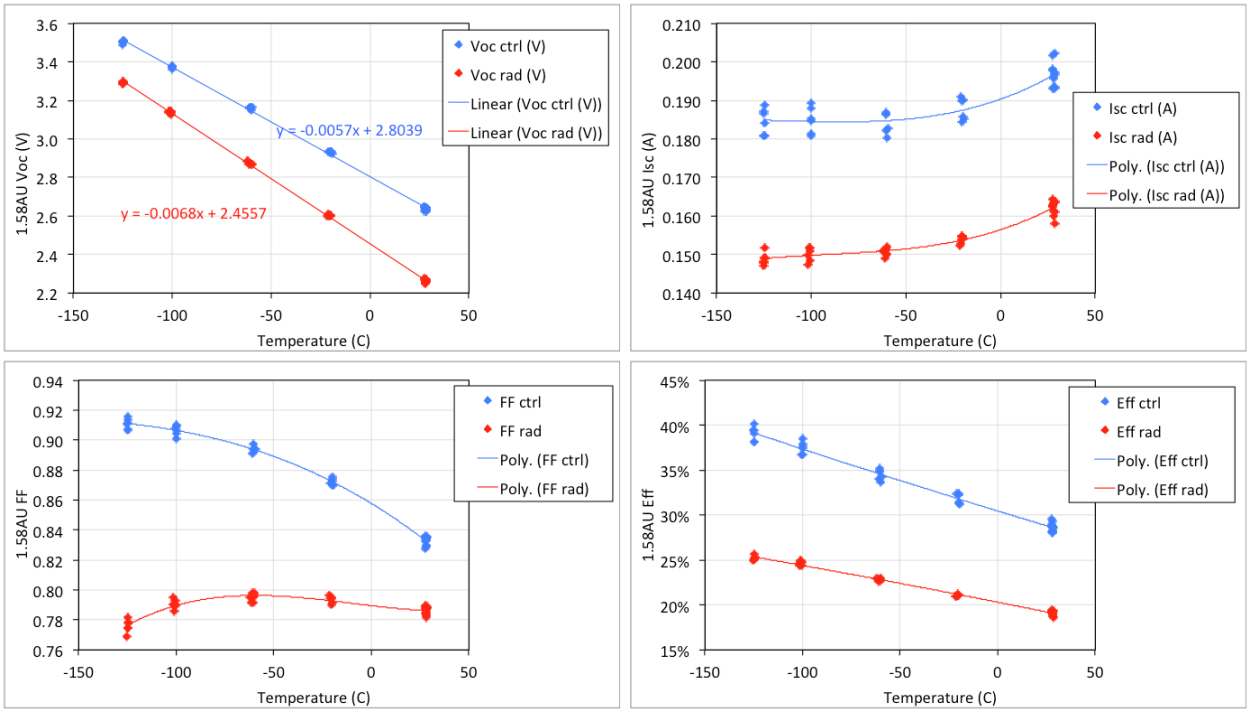

Figure 29. As-measured X25 LIV curve parameters at 1.58AU (10×), on 1st iteration ZTJ unirradiated controls (blue), and test cells irradiated to 4e15 1MeV e^-/cm^2 (red).

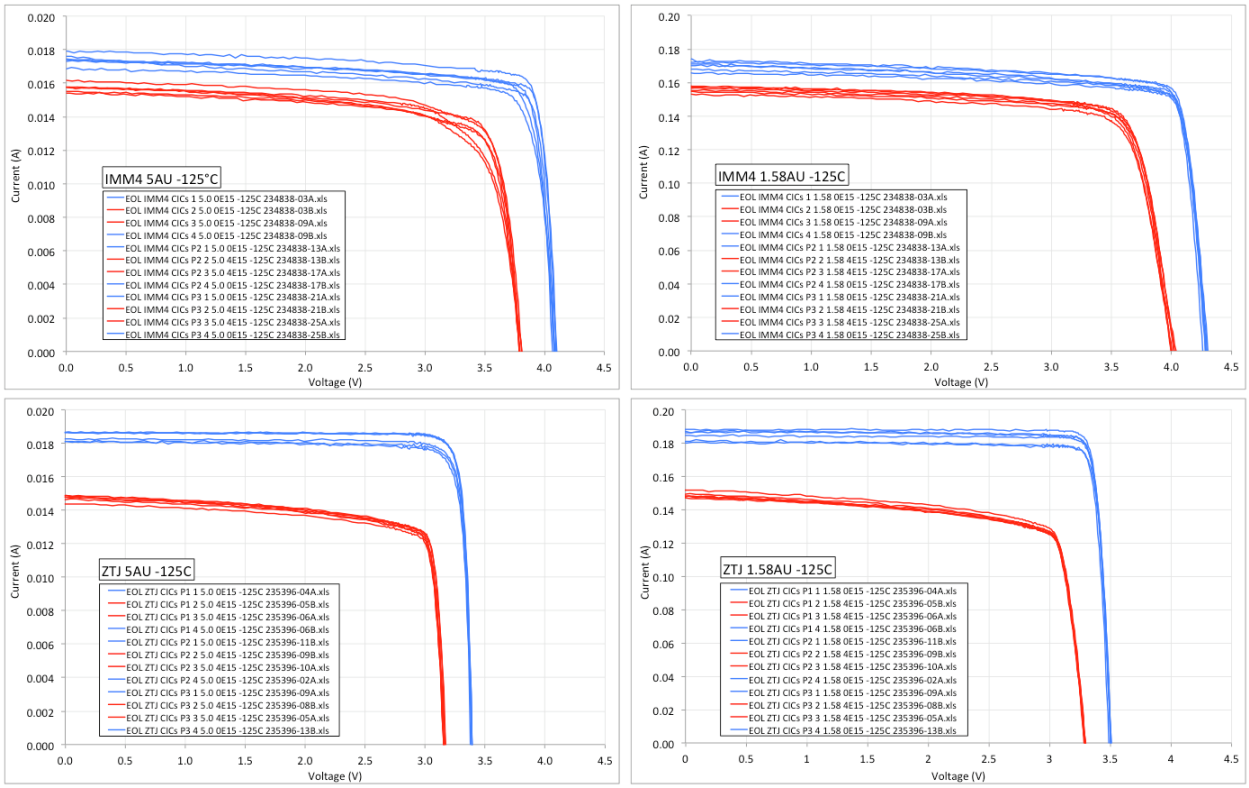

Figure 30. IMM4 and ZTJ 1st-iteration LILT X25 LIV curves at -125°C, 5AU and 1.58AU. Unirradiated control cell data is in blue; irradiated test cell data is in red.

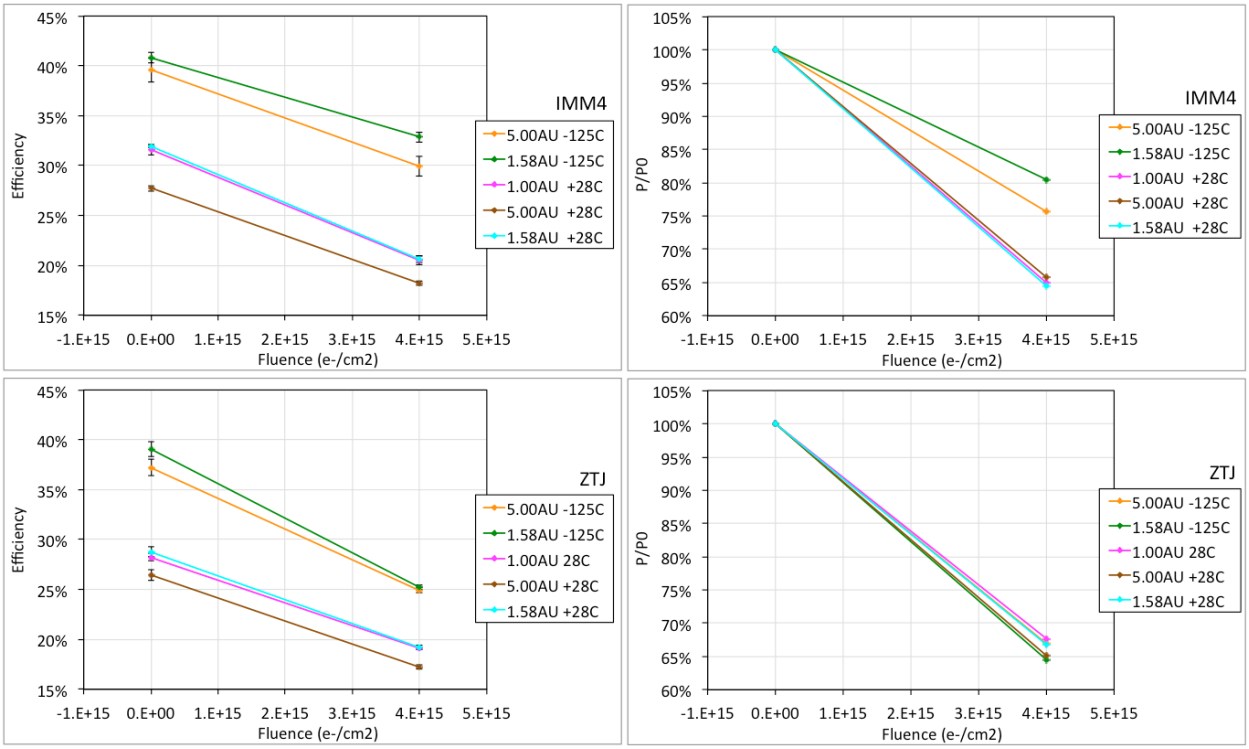

Figure 31. As-measured X25 data on efficiency and remaining power fraction of IMM4 and ZTJ 1st-iteration CICs at +28°C and -125°C, as a function of radiation fluence.

	Fluence (e^-/cm^2)	Efficiency 5AU -125°C	Efficiency 1.58AU -125°C	Efficiency 1AU 28°C
IMM4	0e00 (Ctrl)	39.6% ± 1.2%	40.8% ± 0.5%	31.6% ± 0.5%
	4e15 (Rad)	29.9% ± 1.0%	32.9% ± 0.5%	20.5% ± 0.4%
ZTJ	0e00 (Ctrl)	37.2% ± 0.8%	39.1% ± 0.7%	28.2% ± 0.4%
	4e15 (Rad)	24.9% ± 0.3%	25.2% ± 0.2%	19.1% ± 0.1%

Table 14. As-measured X25 efficiency data on 1st iteration IMM4 and ZTJ, also shown in Fig. 31.

The performance data at -125°C and +28°C is compiled in Figure 31, which shows the as-measured efficiency values and the remaining power fractions for 1st iteration IMM4 and ZTJ. The same efficiency data is also listed in Table 14. The error bars represent one standard deviation over the measured data for the sample population of 6 BOL control CICs and 6 EOL test CICs, for each device architecture. We note that, consistent with our observation for the 0th iteration, the remaining power fraction for IMM4 after irradiation is significantly higher at -125°C than at +28°C. For example: at 5AU, $P/P_0 \approx 0.76$ at -125°C, versus $P/P_0 \approx 0.66$ at +28°C for IMM4. By contrast, the remaining power fraction for ZTJ does not vary as significantly over that same temperature range. For example: at 5AU, $P/P_0 \approx 0.67$ at -125°C, versus $P/P_0 \approx 0.65$ at +28°C for ZTJ. Therefore, the data indicates that the low-temperature post-radiation power retention of IMM4 is superior to that of ZTJ. A low operating temperature is beneficial to the performance of both cell types, however in the case of IMM4 there is an additional boost from increased radiation hardness. This finding suggests that the raised operating temperatures that can be expected under concentration may in fact be detrimental to system performance in the high-radiation environment of interest.

All the 1st-iteration cell types have their grid design optimized for 5AU, which is sub-optimal at 1AU; this explains why the efficiencies listed in the last column of Table 14 are consistently lower than the datasheet efficiencies published for the 1AU-optimized products.

	Fluence (e^-/cm^2)	As-measured	Corrected	NRA goal
IMM4	0e00 (BOL)	39.6% ± 1.2%	37.9% ± 1.2%	35.0%
	4e15 (EOL)	29.9% ± 1.0%	29.5% ± 1.0%	28.0%
ZTJ	0e00 (BOL)	37.2% ± 0.8%	36.8% ± 0.8%	35.0%
	4e15 (EOL)	24.9% ± 0.3%	24.6% ± 0.3%	28.0%

Table 15. LILT (5AU -125°C) efficiency summary for the 1st-iteration IMM4 and ZTJ cells.

The 1st-iteration LILT data shown so far in this report was taken under JPL's X25, which is a 2-zone simulator. As mentioned before, such a simulator is most suitable for testing state-of-

practice triple-junction devices such as ZTJ, but it is not ideal for advanced 4-junction devices such as IMM4. After completing the post-radiation data acquisition, all the 1st-iteration IMM4 samples were re-tested at 28°C 1AU and 5AU on SolAero's SS08 4-zone simulator. Similar to the adjustment we did on the 0th-iteration data, we used the X25 ÷ SS08 efficiency ratios at 28°C as correction factors on the LILT test data, the result of which is summarized in Table 15. An analogous operation was performed on the ZTJ data, however the extent of the correction is much smaller since the JPL and SolAero simulators used for testing ZTJ are both 2-zone. Based on the corrected data for both cell types, we conclude that 1st-iteration IMM4 meets the cell efficiency LILT goals at both BOL and EOL, whereas 1st-iteration ZTJ only meets the BOL target but falls short at EOL.

Accuracy confirmation

As a check of the accuracy of the 28°C-to-LILT correction method outlined in the previous subsection, we decided to retest all 1st-iteration IMM4 samples at LILT (both the BOL unirradiated controls and the EOL irradiated test cells) using SolAero's SS08 4-zone solar simulator and their newly developed LILT test chamber. In that setup, thermal control of the test articles is achieved by permanently bonding them onto aluminum substrates. After completing the 28°C characterization, SolAero integrated all 12 CICs into two-cell coupons for LILT testing, each such coupon containing one unirradiated control and one irradiated test cell. The coupons were tested as a function of temperature between +28°C and -125°C, under 5AU irradiance calibrated to AM0 in all four spectral zones relevant to IMM4. The -125°C average and standard deviation results are shown in Table 16, in the "SS08 (4-zone) as-measured" column.

Fluence (1MeV e^-/cm^2)	X25 (2-zone) corrected	SS08 (4-zone) as-measured	NRA goal
0e00 (BOL)	37.9% ± 1.2%	37.9% ± 0.2%	35.0%
4e15 (EOL)	29.5% ± 1.0%	30.1% ± 0.7%	28.0%

Table 16. Efficiency comparison between X25 2-zone corrected data versus SS08 4-zone as-measured data, on 1st-iteration IMM4 CICs tested at 5AU -125°C.

Note that there is very good agreement at both BOL and EOL LILT, to within measurement error, between the corrected X25 2-zone data, and the raw as-measured SS08 4-zone data. This confirms the accuracy of the corrected X25 results. Most importantly, it confirms that the 1st-iteration IMM4 design does meet both the BOL and the EOL LILT efficiency objectives, with significant margin, even in the absence of concentration.

The EOL current balance among the subcells of the 1st-iteration IMM4 design was investigated at SolAero through a spectrally-enhanced LIV measurement on one of the irradiated CICs. One LIV curve was measured under the standard AM0 calibration for the SS08 4-zone simulator; and four additional LIV curves were tested under boosted spectra having >13% additional irradiance in only the spectral range relevant to J1, J2, J3 or J4 respectively, as determined from the current output of the corresponding isotype calibration cells. The efficiency boost obtained from flooding each of the four individual junctions informs the design direction for the 2nd cell

iteration. The results are consistent with the temperature-dependent EQE current-balance data mentioned in the previous subsection.

Cell architecture trade

Upon completion of the X25 data acquisition for the 1st cell design iteration, a cell architecture trade study was performed, which downselected between the IMM4 and the ZTJ device structures. This subsection details the items that were considered as part of that trade.

(1) LILT BOL efficiency. Table 18 summarizes the X25 corrected average and standard deviation efficiency data for IMM4 and ZTJ based on the 1st design iteration, under various test conditions relevant to meeting the LILT BOL target. Without exact knowledge of the concentrator array design, one cannot predict the exact cell operating temperature under concentration. However, we note that a planar array at a 1.58AU sun distance would operate at approximately -20°C, which places a conservative upper bound on the operating temperature for a 10× concentrator system at 5AU, and is shown in the table only in order to bracket the comparison between IMM4 and ZTJ. Overall, IMM4 has a slight performance advantage over ZTJ at LILT BOL.

Test conditions	ZTJ	IMM4	IMM4/ZTJ ratio
5AU -125°C	36.8% ± 0.8%	37.9% ± 1.2%	103%
1.58AU (10×) -125°C	38.6% ± 0.7%	39.1% ± 0.5%	101%
1.58AU (10×) -20°C	31.5% ± 0.5%	34.7% ± 0.4%	110%

Table 18. LILT BOL efficiency comparison between ZTJ and IMM4.

(2) LILT EOL efficiency. Table 19 summarizes the X25 corrected average and standard deviation efficiency data for IMM4 and ZTJ based on the 1st design iteration, under various test conditions relevant to meeting the LILT EOL target. Analogously to the BOL case, the 1.58AU -20°C row is only shown as a way to bracket the relevant test conditions. Therefore, in the case of LILT EOL, IMM4 has a very substantial performance advantage over ZTJ, as evidenced by the "IMM4/ZTJ ratio" column.

Test conditions	ZTJ	IMM4	IMM4/ZTJ ratio
5AU -125°C	24.6% ± 0.3%	29.5% ± 1.0%	120%
1.58AU (10×) -125°C	24.9% ± 0.2%	32.4% ± 0.5%	130%
1.58AU (10×) -20°C	20.8% ± 0.1%	23.9% ± 0.4%	115%

Table 19. LILT EOL efficiency comparison between ZTJ and IMM4.

(3) Mass. The CIC-level areal mass densities for IMM4 and ZTJ are summarized in Table 20. CIC mass is an important consideration, because it factors into meeting the array-level specific power target. For both cell types, further mass reductions are possible by thinning the substrate, which would be at the expense of some radiation shielding; this can be beneficial in those cases where the array structure already provides sufficient shielding. In either case, the IMM4 CIC has a very substantial mass advantage over ZTJ.

Component mass	ZTJ	IMM4	ZTJ/IMM4 ratio
CIC (kg/m^2)	1.18	0.91	129%

Table 20. CIC-level areal mass density comparison between ZTJ and IMM4.

(4) Further potential. Based on the 1st iteration, we have determined that the performance of IMM4 can be further improved through subsequent design optimization and development. For example, optimizing the current balance for EOL may further increase the efficiency margin of IMM4 over the target. By contrast, we do not see significant opportunities for further improving the performance of ZTJ; and most importantly, we see no clear path for ZTJ to meet the LILT EOL efficiency objective, which it falls short of. Therefore, IMM4 has the advantage over ZTJ, when it comes to potential for further improvement.

(5) Maturity and risk. Table 21 summarizes the technology readiness of IMM4 versus ZTJ. The ZTJ technology has been powering spacecraft at 1AU since 2009, and is baselined for power production at LILT on the solar array for the Europa Clipper mission. By contrast, IMM4 has only flown at 1AU in technology demonstration missions so far; the IMM4 design that results from EESP cell development, to be completed in Option I, will also fly on Europa, once again as a technology demonstration and in-situ LILT characterization experiment. Therefore, we believe that ZTJ has the advantage over IMM4, in terms of maturity.

Environment	ZTJ	IMM4
1AU, at present	TRL 9	TRL 7
LILT, at present	TRL 5	TRL 5
LILT, after Europa (projected)	TRL 9	TRL 7

Table 21. Technology readiness comparison between ZTJ and IMM4.

Table 22 is the trade matrix which summarizes the scoring for each of the two cell architectures in the above-mentioned categories. All scores are on a scale of 1-10. Based on this trade study, IMM4 was selected as the cell technology for EESP going forward.

Category	Weight	ZTJ score	IMM4 score
(1) BOL efficiency	10%	9	9
(2) EOL efficiency	30%	4	9
(3) CIC mass	30%	6	9
(4) Potential	20%	3	8
(5) Maturity	10%	8	7
Weighted score		**5.3**	**8.6**

Table 22. Trade matrix for downselecting between the ZTJ and IMM4 device architectures.

Array-structure concept trade

Upon completion of the IMM4-versus-ZTJ downselect, an array-structure trade study was performed, which downselected between the planar and the concentrator concepts. This subsection details the items that were taken into consideration as part of that trade.

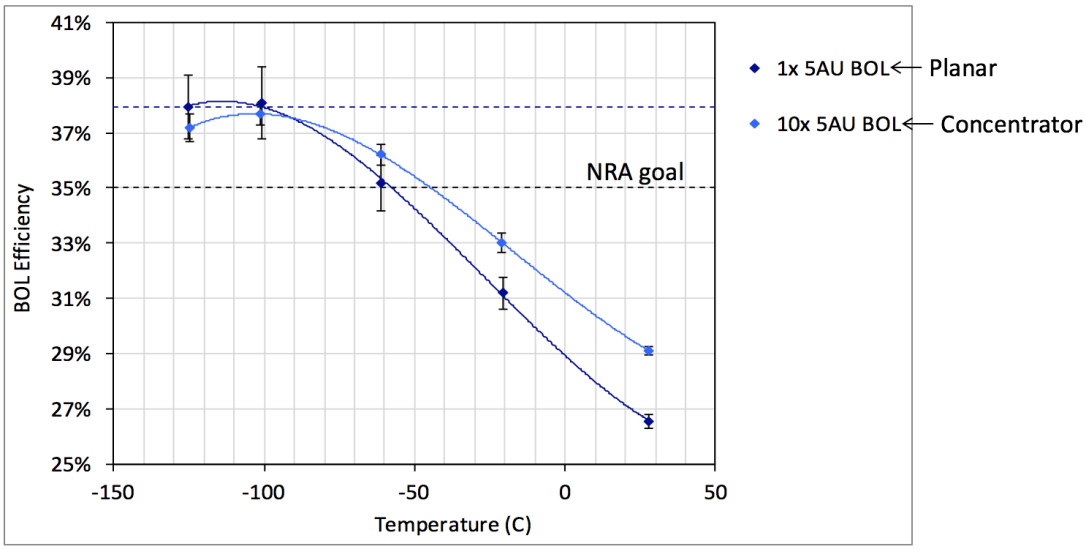

Figure 33. Corrected X25 BOL IMM4 efficiency data based on the 1st design iteration, for a planar array (1×); and for a concentrator (10×) assuming 95% optical efficiency.

(1) LILT BOL cell efficiency. Figure 33 shows the corrected X25 IMM4 1st-iteration BOL data taken at 5AU and 1.58AU, as a function of temperature. The markers represent average data, and the error bars are standard deviations over the measured cell population. The 1× 5AU data is shown in the darker shade of blue, and it represents the cell efficiency we can expect in a planar array; at 5AU, the operating temperature is expected to be close to -125°C, and the blue dashed line represents the 5AU -125°C efficiency for the planar case. The black dashed line represents the 35% LILT BOL efficiency objective. The 10× 5AU data is shown in the lighter shade of blue, and it represents the 1.58AU data, which corresponds to a 10× concentrator with respect to ambient irradiance at 5AU; the corrected 1.58AU efficiency data was multiplied by a factor of 0.95, which is an optimistic estimate of the optical efficiency that would be attainable at BOL in a concentrator system. For comparison, the Scarlet concentrator array has 89% optical efficiency; and the ATK CellSaver array has a 93-96% optical efficiency. Both planar and concentrator systems have the capability of exceeding the LILT BOL cell efficiency target. Note however that at all temperatures, the 10× curve falls below the blue dashed line; this means that, regardless of the cell operating temperature in the concentrator system, the cell efficiency will be higher in a planar system operating at 5× -125°C. However, the performance advantage for the planar case only becomes substantial when the cell temperature for the concentrator case is greater than ~-80°C. Overall, we estimate that the planar concept offers a slight advantage over the concentrator, in terms of LILT BOL cell efficiency.

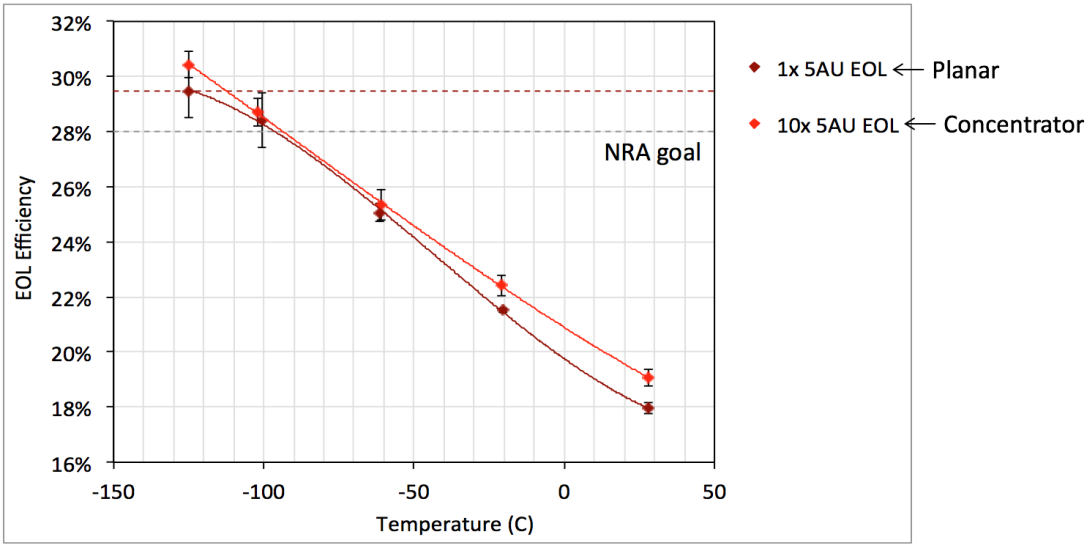

Figure 34. Corrected X25 EOL efficiency IMM4 data based on the 1st design iteration, for a planar array (1×); and for a concentrator (10×) assuming 94% optical efficiency.

(2) LILT EOL cell efficiency. Figure 34 shows the corrected X25 IMM4 1st-iteration EOL data taken at 5AU and 1.58AU, as a function of temperature. As before, the markers represent average data, and the error bars are standard deviations over the measured cell population. The 1× 5AU data is shown in the darker shade of red, and it represents the cell efficiency we can expect in a planar array; at 5AU, the operating temperature is expected to be close to -125°C, and the red dashed line represents the 5AU -125°C efficiency for the planar case. The black dashed line represents the 28% LILT EOL efficiency objective. The 10× 5AU data is shown in the lighter shade of red, and it represents the 1.58AU data, which corresponds to a 10× concentrator with respect to ambient irradiance at 5AU; the corrected 1.58AU efficiency data was multiplied by a factor of 0.94, which represents an aggressively optimistic estimate of the optical efficiencies that would be attainable in a concentrator system at EOL. For comparison, the CellSaver concentrator array has 85% EOL optical efficiency. Both planar and concentrator systems have the capability of exceeding the LILT EOL cell efficiency target. Without knowing the exact details of the concentrator heat spreading approach, it is not possible to predict the exact cell operating temperature in the concentrator. If the cell operating temperature in the concentrator case is less than ~-120°C, there may be a slight performance advantage over the planar case operating at -125°C, although not a significant one given the error bars on the data; and, the reverse is true if the temperature under concentration is greater than ~-100°C. Overall, we estimate that the concentrator concept may offer a slight advantage over the planar one, in terms of LILT EOL cell efficiency.

(3) Specific power. Table 23 estimates the array-level specific power for a planar and concentrator design. Without knowing the exact concentrator design, it is not possible to accurately estimate the areal add-on mass savings that lighter-weight optics and smaller area CICs can offer over having the same surface entirely populated with CICs. For the purposes of the comparison, we estimate that the concentrator can reduce the CIC-level add-on mass by a factor of ~2; for reference, the Stretched Lens Array does claim this level of mass savings, albeit with respect to heavier, state-of-practice CICs which makes the mass savings easier to achieve

in a relative sense. Both the planar and the concentrator options can meet the EESP 8-10 W/kg LILT EOL specific power objective. However, depending on the design, the concentrator option may do so with higher margin. We therefore estimate that the concentrator concept has some advantage over planar, as far as specific power is concerned.

Assumption	Planar	Concentrator
Electrical/optical mass (kg/m^2)	0.91	0.46
Mechanical mass (kg/m^2)	0.72	0.72
Total-area packing factor	0.80	0.80
LILT EOL cell efficiency	28%	28%
LILT EOL Array Specific Power (W/kg)	**8.5**	**11.3**

Table 23. Assumptions for estimating specific power for a planar versus a concentrator array.

(4) Development risk. Planar array-structure designs already exist that are at TRL5 for LILT environments, such as for example the ATK UltraFlex/MegaFlex (which was in fact selected as the preferred technology going forward, subsequent to the completion of this trade). Therefore, the development risk for a planar system is expected to be low. By contrast, we do not know of any concentrator systems that would be as far along in terms of development. Concentrator systems are necessarily more complex in design, meaning that there are more components which can introduce unexpected challenges during the development process. Furthermore, concentrator systems have a greater number of critical functions that would need to be demonstrated during the development process, for example: optical efficiency as a function of radiation exposure; deployment and stability of optical assemblies; optical alignment as a function of temperature; the effect of outgassing and other life effects on the performance and reliability of the system; etc. As such, the development risk is relatively high in the case of the concentrator. We therefore find that the planar concept has a significant development-risk advantage over the concentrator one.

(5) Mission risk. Depending on the exact design (in particular, on the concentration ratio), concentrator systems will place more stringent pointing requirements on the spacecraft, which may result in increased mission cost. Also, concentrator systems have higher vulnerability to micrometeorites, since losing one cell leads to more than one cell's worth of power loss, by a factor equal to the concentration ratio. Deep-space mission design often includes Venus fly-bys, during which planar arrays are typically tilted off-sun to control their temperature; in the case of concentrators, such an approach may not be viable, placing additional constraints on mission design. Therefore, we assess that while the mission risk from planar array systems is low, in the case of concentrator systems this risk is higher. Overall, the planar concept does offer a non-negligible advantage over the concentrator, when it comes to mission risk.

(6) Development cost. Due to the availability of several medium-TRL options, we estimate that the development required for developing a planar array structure for the EESP environment would be minimal, as would be the associated development cost. Therefore, choosing a planar array structure would allow us to allocate more resources to further cell development, which would reduce the overall risk at the system level. By contrast, we expect concentrator

structures to require significant development, resulting in high development cost. This means that in terms of development cost there is a clear advantage for planar over concentrator.

(7) Mission cost. The cost of the solar cells is expected to dominate the cost of the electrical add-on components for the solar array. In comparison, optical components are expected to be relatively cheaper. Therefore, the cost of the flight build is expected to be lower for a concentrator array as compared to a planar one. In addition, the higher specific power expected of concentrator systems should also lead to lower cost. However, flight acceptance testing is expected to be more costly in the case of a concentrator system, which would require e.g. large-area collimated light sources, stability in 1g, and likely a larger, more complex test suite. For reference, both the CellSaver and the Stretched Lens Array claim $/W savings over a planar approach. Overall, we assess that a concentrator array should have a non-negligible mission-cost advantage over the planar option.

Table 24 is the trade matrix which summarizes the scoring for each of the two array-structure concepts in the above-mentioned categories. All scores are on a scale of 1-10. Note that for all categories, a quantitatively exact comparison would require knowledge of the particular concentrator design; however, in making the estimated comparisons in each category, we have endeavored to use as optimistic assumptions for the concentrator case as we could reasonably conceive of. Based on this trade study, the planar concept was selected as the array structure for EESP going forward.

Category	Sub-category	Weight	Planar score	Concentrator score
Performance	(1) LILT BOL cell efficiency	10%	9	8
	(2) LILT EOL cell efficiency	15%	8	9
	(3) LILT EOL array specific power	20%	8	9
Risk	(4) Development risk	20%	9	5
	(5) Mission risk	15%	9	7
Cost	(6) Development cost	10%	10	5
	(7) Mission cost	10%	7	9
Weighted score			**8.6**	**7.4**

Table 24. Trade matrix for downselecting between the planar and concentrator concepts.

Array-structure RFI

Subsequent to the cell architecture and array-structure concept downselects, we proceeded to work on the selection of a particular lightweight planar scalable array-structure technology, from amongst the products currently available from various vendors. A request for information (RFI) was sent out to five recipients, namely: Orbital ATK, DSS, SolAero, Boeing, and Lockheed

Martin. The information submitted to the RFI recipients included the CIC-level areal mass and the LILT BOL and EOL performance of the solar cell; the requirement that the array structure shall be a planar lightweight scalable array; and the statement of work (SoW) for the array-partner portion of the planned Option I effort. The information requested by the RFI was: a design description for a solar array capable of ≥5kW at LILT EOL; a compliance matrix with respect to the EESP NRA goals; current-TRL assessment and supporting evidence, while emphasizing particular interest in technologies that have TRL ≥5 for the EESP environment; and ROM price for the array-structure portion of the Option I work, based on the provided SoW.

Responses to the RFI were received from Orbital ATK, DSS, SolAero and Lockheed Martin. Based on evaluation of these responses, we selected MegaFlex from Orbital ATK as the array-structure technology for JPL's EESP project. As detailed in the "Technical description" section of this report, MegaFlex enables the array system to meet nearly all EESP goals without the need for development on the array-structure alone. Also, as detailed in the TRL assessment section below, MegaFlex is currently at TRL6 for 1AU environments, and at TRL5 for LILT. In addition, there is already some, albeit limited experience for integrating IMM4 CICs with MegaFlex substrates at the array coupon level. We therefore found MegaFlex to be the most suitable array-structure technology for meeting the performance objectives and system-level TRL timetable of this project.

Related developments

In this subsection, we highlight two recent developments from other projects, which may have beneficial future impacts on JPL's EESP task.

The first development of interest is that the Europa Clipper project is now planning to fly LILT-optimized IMM4 cells of the design that eventually emerges from EESP, as a technology demonstration project to be included on the Clipper spacecraft. There will be a total of 5 IMM4 cells, one on every other panel of the solar array. And, each of these IMM4 cell will be connected to power subsystem electronics that will periodically sweep and measure its LIV curve, thereby obtaining telemetry data on the in-flight performance of this technology in the relevant environment. Once completed, this technology demonstration project will bring JPL's EESP cell component to TRL-7, which is a critical and often challenging milestone on the path to flight infusion.

The second development of interest is that JPL has allocated internal FY17 funding to upgrading our solar simulator equipment. A new simulator will be procured with enhanced spectral tunability of at least 5 zones, making it suitable for precise characterization of IMM4 devices without the need for corrections. While the procurement effort is still in its planning stages, it is nevertheless a promising development, since adding 4-zone tunability to the LILT setup will significantly simplify the EESP test sequence during the Option periods.

Performance quantification

For an estimate of the system-level performance, based on the data demonstrated to date, please see the "Technical description" section above.

Proposed system concept

System concept overview

The proposed array system is an integration of advanced-architecture solar cells with lightweight scalable array structures. The solar cell component is an ultra-high efficiency IMM4 device, featuring a modified design that enables optimal performance in low irradiance, low temperature and high-radiation (LILT/Rad) environments. The array structure component is MegaFlex, a planar lightweight large-scale flexible blanket.

Current TRL assessment

For the purposes of the TRL assessment in this section, the relevant environment is taken to be the EESP environment as detailed in the NRA, specifically: LILT conditions of 5AU -125°C; EOL accumulated radiation dose of 4e15 1MeV e-/cm^2; 100-300V operating voltage; and Xe plasma fields of 2eV electron temperature and 1e8/cm^3 number density. Other environments such as 1AU or the Mars surface are not considered to be the relevant environment and are only cited in the TRL assessment in those cases where the exact space environment is expected to have little or no effect on component or system functionality.

(1) TRL assessment for CIC component. The IMM4 coverglassed interconnected cell (CIC) technology has been validated in the relevant environment. We therefore assess that the IMM4 CIC technology is now at TRL5. Specifically, as detailed in the "Base period results" section, a quantity of 36 IMM4 CICs were tested in the laboratory under LILT conditions of 5AU -125°C; furthermore, a quantity of 12 IMM4 CICs were tested at LILT after exposure to an EOL radiation dose. The critical function of the CIC is its power-conversion efficiency at LILT BOL and at LILT EOL, which was demonstrated to meet the performance objectives as shown in Table 2. Therefore, all sub-components making up the CIC test articles were also implicitly validated through these tests, specifically: the IMM4 solar cell device; Ag-clad Kovar welded interconnects; DC93-500 optically transparent coverglass adhesive; and the 0.004"-thick AR-coated CMG coverglass. The CICs tested during the Base period did not contain silicon bypass diodes, however such diodes had been validated previously, as part of ZTJ CIC testing for the Europa Clipper development project, which has similar environmental requirements (5.5AU, -140°C, 4e15 1MeV e-/cm^2).

(2) TRL assessment for array-structure component. The MegaFlex array-structure technology has been validated in the relevant environment at the brassboard level. The critical function of the structure is to serve as a mechanical substrate for the solar cells. As demonstrated by analysis in the "Technical description" section, this structure technology supports the array system towards meeting its goals for mass and volume. In addition, the NASA 1AU SEP development project has demonstrated by test that the MegaFlex array structure supports the array-system functionality when it comes to plasma and high-voltage operation.

The Europa Clipper mission performed a pre-Phase-A feasibility study on the UltraFlex array structure, which is a precursor technology sharing a large fraction of components and functionality with MegaFlex. This study included performance, functional and thermal cycling testing at the coupon level; and thermal, power, radiation and structural analyses at the array

level. The study found that the UltraFlex structure is fully viable for the LILT and radiation environment of Europa Clipper, which is very similar to that of EESP.

In addition, the NASA 1AU SEP technology development project completed on MegaFlex has performed deployment testing at the wing demonstration unit level; structural and scalability analyses at the array level; and also ESD and thermal cycling testing at the coupon level. Figure 36 is an excerpt from Carolyn Mercer's paper "SEP Technology: Development for Electric Propulsion" presented at the 33rd Space Power Workshop in 2015, summarizing the wing- and array-level tests and analyses that were performed as part of that project. In addition, ESD testing performed in JPL's plasma lab as part of the same SEP technology development project, demonstrated that the MegaFlex structure supports the array system in meeting its high-voltage and plasma operation requirements.

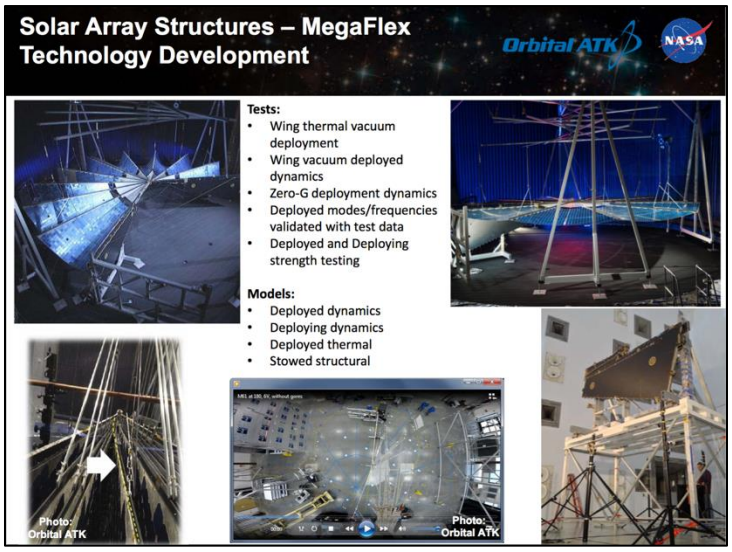

Figure 36. Summary of tests and analyses performed on the MegaFlex demonstration unit (MDU) and array as part of NASA's 1AU SEP technology development project.

The MegaFlex array-structure technology has not been flown yet, although its precursor technology UltraFlex does have flight heritage at 1AU from the Cygnus CRS program, as well as from the Phoenix lander on the Mars surface. In addition, the UltraFlex/MegaFlex platform has been baselined for the Lucy mission to the Jupiter Trojans, which at 5.3AU is to fly in a LILT environment similar to EESP.

Based on the evidence outlined above, we conclude that the current readiness level for the MegaFlex structure component in the EESP environment is TRL5.

(3) TRL assessment for array system. The EESP array system, which integrates the LILT and radiation-optimized IMM4 CIC with the MegaFlex structure, has been validated at the breadboard level in a laboratory environment. The critical function of the array system is its power production capability. As detailed in the "Technical description" section, this function has been demonstrated by analysis to meet the EESP objective for specific power. In addition, the NASA 1AU SEP technology development project has performed ESD and thermal cycling testing on a MegaFlex coupon integrated with 1AU-optimized IMM4 CICs, under temperature ranges and current leakage requirements relevant to 1AU environmental conditions. Based on

this evidence, we conclude that the current readiness level for the proposed array system in the EESP environment is TRL4.

TRL5 feasibility

The array system will be validated at the brassboard level in the relevant environment during the Option I period, thereby bringing the system-level readiness to TRL5. A small-scale but otherwise representative array coupon will be built and tested during the Option I period.

We estimate the feasibility of developing this technology to TRL5 during Option I to be high, based on the fact that the constituent parts (the CIC and the structure) have both been successfully developed to high TRLs for other environments. Specifically, the IMM4 cell has flown at 1AU in technology demonstration experiments such as MISSE; also, IMM4 cells will partially power the 1AU OTB satellite, launching 2017. Therefore, for 1AU applications, the cell technology is currently at TRL7, and expected to reach TRL9 later this year. Similarly, the MegaFlex array-structure technology has been developed by NASA to TRL6 for 1AU SEP applications, and the similar UltraFlex has supplied power to the Cygnus ISS resupply spacecraft also at 1AU, as well as to the Phoenix lander on the surface of Mars. Importantly, MegaFlex has demonstrated by test the capability to function in thruster plume plasma environments at 1AU. Therefore, for 1-2AU applications, the array-structure technology is currently at TRL6-9.

Another reason for having high confidence in the feasibility of achieving system-level TRL5 during Option I is the fact that the constituent parts are already at TRL5 individually. As detailed in the "Current TRL assessment" section above, both the cell and the array structure have now been validated in the relevant EESP environment. When the array concept was first proposed, the IMM4 cell was at TRL3, making it the lowest-TRL component in the system, and the highest risk to advancing the system-level TRL. Therefore, now that the cell readiness level has been significantly advanced, the risk to the feasibility of system-level TRL5 has been substantially reduced. What remains to be validated is the ability to integrate the cell and structure technologies so as to meet system-level requirements in the relevant environment.

Beyond Option I, the array system will be further validated at the subsystem level in the relevant environment, by building and testing a high-fidelity prototype panel during Option II. Upon completion of the EESP development, the system-level readiness for the EESP environment is projected to reach TRL5+.

Scalability

The solar cells for the EESP array will be made with the same fabrication techniques as SolAero's 1AU-optimized IMM cell products, albeit with design changes requiring different growth recipes or grid mask designs. Therefore, we expect that the scalability of the fabrication process will remain unaffected, leveraging SolAero's infrastructure and experience in the high-volume manufacturing of multijunction cells for space applications. Also, design scalability is not a concern, since to populate a very large-area solar array, one simply scales up the quantity of solar cells in the build.

For the array structure, the MegaFlex technology has demonstrated design and manufacturing scalability up to 450kW 1AU BOL power levels, which when combined with the EESP-optimized

IMM4 cell would translate into LILT EOL power levels of 15kW, well in excess of the 5kW objective. As part of NASA's SEP technology development project, MegaFlex has showed viability in terms of design, test and manufacturing capabilities, with the 17.8m-diameter wing design for EESP being only mid-range for these analyses.

Current TRL summary

The current TRL assessment for the array system and constituent components, which was detailed in this section, is summarized in Figure 41.

	Green - TRL 4, 5, 6, 7, 8, 9
	Yellow - TRL 3
	Red - Below TRL 3
	White - Unknown
X	Exists
Y	Yes
N	No
?	Uncertain

System, Component, Subsystem	Demonstration Unit: Component	Demonstration Unit: Breadboard	Demonstration Unit: Prototype	Demonstration Unit: Flight Qualified	Environment: Laboratory Environment	Environment: Relevant Environment	Environment: Space Environment	Environment: Operational Environment (Launch/Space)	Analytical Scalability	Manufacturing Scalability	Overall TRL	Rationale for Overall TRL
System: Solar Array		Y			Y						4	NASA SEP Megaflex+IMM4 coupon test
Component: IMM4 CIC	Y					Y					5	EESP IMM4 and Europa ZTJ CIC tests
Component: MegaFlex Structure		Y				Y					5	Europa Pre-Phase-A test and analysis

Figure 41. TRL assessment summary for the proposed solar array system and components.

Risk assessment

The project has identified 10 risks, whose status is summarized in Figure 42. The initial status is as of the time of the proposal submission in October 2015, whereas the current status is as of the end of the Base period, April 2017. The projects listed in gray font have been retired. The sub-sections below provide further details on each of the project risks and their current status.

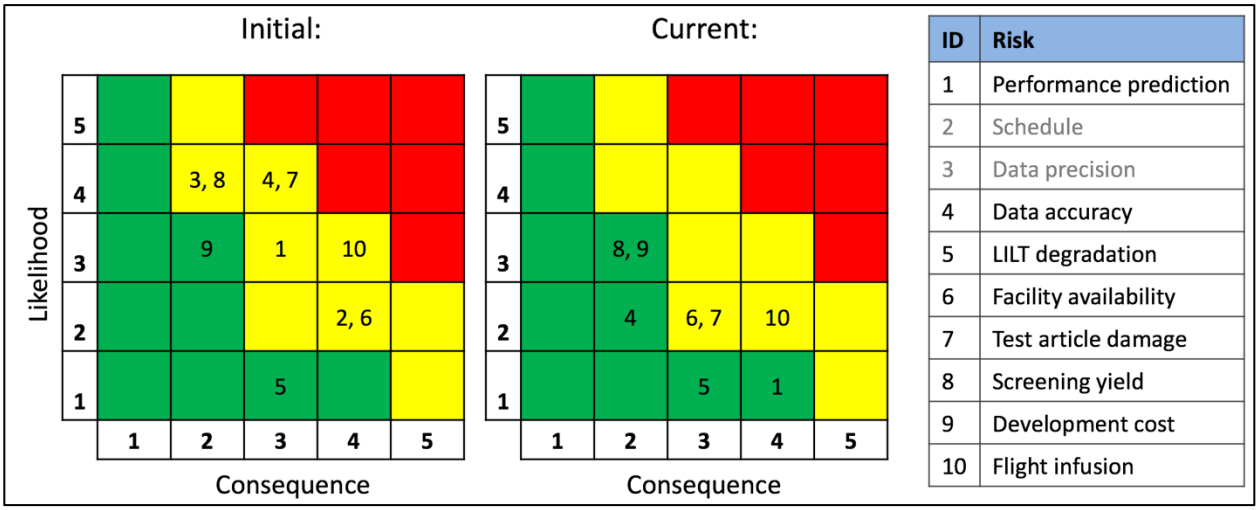

ID	Risk
1	Performance prediction
2	Schedule
3	Data precision
4	Data accuracy
5	LILT degradation
6	Facility availability
7	Test article damage
8	Screening yield
9	Development cost
10	Flight infusion

Figure 42. Initial (Oct-2015, proposal) and current (Apr-2017, end of Base period) risk status.

Risk #1: Performance Prediction

Risk statement:
If the model predicting LILT and radiation-optimized cell efficiency at the conclusion of development is incorrect, the project may not meet its objectives at the cell level.

Context:
At the time of the proposal, no LILT data existed yet on IMM4, and only limited LILT data existed on ZTJ. Performance predictions at that time were based on 1AU test data and modeling.

Initial likelihood (1-5): 3
Similarity to ZTJ and optimal spectrum splitting make IMM4 a likely good LILT performer; however, low-level shunts in the metamorphic subcells are a possible issue.

Initial consequence (1-5): 3
The project may still meet its array-level performance goals by use of a concentrator approach.

Timeframe:
Base and Option I periods.

Mitigation strategies:
(1) Test-driven development plan, with ~4 design and test iterations;
(2) Multiple cell architectures and array concepts being considered in parallel.

Status:
At the conclusion of the Base period, IMM4 meets the NRA goals for LILT cell efficiency. Further development will increase margin for manufacturing scalability.

Current likelihood (1-5): 1
Reduced. Performance data has been consistent with predictions. We expect to retire this risk upon completion of cell development iterations 2-4 and design freeze at the end of Option I.

Current consequence (1-5): 4
Increased. The planar array concept has been selected, removing the possibility of concentration as an avenue for boosting cell performance.

Risk #2: Schedule

Risk statement:
If subcontract setup, fabrication and screening, environmental exposures, performance testing, or array partner selection take longer than expected, the work planned for the Base period may not be completed in time.

Context:
The EESP Base period has a short 9-month duration, with limited schedule margin.

Initial likelihood (1-5): 2
The schedule is aggressive but feasible.

Initial consequence (1-5): 4
Not completing all planned work (e.g., fewer cell design iterations) may lead to reduced performance capability by the end of the Base period, and could therefore result in a non-award for Option I.

Timeframe:
Base period.

Mitigation strategies:
(1) Using the X25 and accelerator facilities efficiently by testing and irradiating multiple cells at a time;
(2) Transferring cells fabricated on the FY16 R&TD task (no longer in use by that project) to EESP, where they were used in the 0^{th} iteration work;
(3) Performing the cell technology and array-partner downselects as soon as sufficient necessary information had become available.

Status:
The Base period work has been completed as planned, and the cell performance goals have been met.

Current likelihood (1-5): N/A
This risk has been retired.

Current consequence (1-5): N/A
This risk has been retired.

Risk #3: Data Precision

Risk statement:
If test reproducibility is poor, the resulting cell or coupon performance data may have large statistical fluctuations and error bars.

Context:
The Europa Clipper cell test program was struggling with large repeatability error bars during late 2015.

Initial likelihood (1-5): 4
At the time of proposal submission, the X25 simulator test setup had poor stability, e.g. +/-7% relative at LIRT.

Initial consequence (1-5): 2
Large uncertainties in performance estimates may require test articles with higher true performance, which would be more difficult to achieve.

Timeframe:
Base period.

Mitigation strategies:
(1) Solar simulator optics upgrade;
(2) Increased definition for test procedures;
(3) Periodic testing of statistically significant quantities of nominally unchanged controls alongside the test cells.

Status:
The EESP data from the 0^{th} and 1^{st} iterations has demonstrated good precision. We will continue to monitor the process by using controls throughout the remainder of the project.

Current likelihood (1-5): N/A
This risk has been retired.

Current consequence (1-5): N/A
This risk has been retired.

Risk #4: Data Accuracy

Risk statement:
If test data is inaccurate, we may lose the ability to convincingly verify the project requirements.

Context:
Previous round-robin accuracy checks on the X25 simulator yielded satisfactory results for state-of-practice triple-junction UTJ and ZTJ cell technologies, but no information existed yet on the X25's ability to test IMM4.

Initial likelihood (1-5): 4
The X25 is a 2-zone solar simulator which may be inadequate for testing 4-junction devices such as IMM4.

Initial consequence (1-5): 3
Large correction factors would cast doubt on the validity of JPL's cell or coupon performance measurements.

Timeframe:
Base and Option I periods.

Mitigation strategies:
(1) Round-robin comparisons between JPL's X25 2-zone simulator and SolAero's SS08 4-zone simulator at 1AU and 5AU +28°C;
(2) Development of a LILT test chamber at SolAero, to be used with their 4-zone simulator;
(3) Procurement of a 5-zone simulator, to be used as part of JPL's LILT setup.

Status:
The LIRT (5AU +28°C) round robins for the 0th and 1st iterations yielded reasonable correction factors of ~4% BOL and ~1% EOL. The SolAero LILT setup is now functional, and the accuracy of the X25 28°C-based LILT data correction method has been verified for the 1st-iteration IMM4. A 5-zone simulator is planned to be integrated with JPL's LILT setup by September 2017.

Current likelihood (1-5): 2
Reduced, thanks to good agreement between the corrected-X25 and the SS08 LILT data for 1st-iteration IMM4. We plan to retire this risk upon completion of a full-LILT round robin during Option I.

Current consequence (1-5): 2
Reduced, since corrections for the 0th and 1st iterations have been small.

Risk #5: LILT degradation

Risk statement:
If significant LILT performance degradation occurs in IMM4 but cannot be eliminated from the design, cell performance goals may not be met (also see Risk #1).

Context:
Solar cell technologies that were previously investigated have shown performance degradation under LILT test conditions.

Initial likelihood (1-5): 1
Based on past experience, LILT performance-limiting mechanisms can be eliminated through appropriate design modifications.

Initial consequence (1-5): 3
Meeting project goals may be difficult without successfully optimizing the design for LILT and radiation.

Timeframe:
Base and Option I periods.

Mitigation strategies:
(1) Performing multiple build-test-investigate-redesign iterations during the Base and Option I periods, with margin on the expected number of iterations.

Status:
The 0th and 1st design iterations have been completed. IMM4 meets the cell performance goals, however there is room for further improvement, e.g. rebalancing the current for optimal LILT EOL performance.

Current likelihood (1-5): 1
Unchanged. We will retire this risk upon the successful completion of the 3rd design iteration.

Current consequence (1-5): 3
Unchanged.

Risk #6: Facility Availability

Risk statement:
If the fabrication, test and exposure facilities or equipment are not available exactly when needed, delays may be introduced into the project schedule.

Context:
The SolAero fab, X25 lab, Dynamitron facility, Plasma lab and OATK thermal cycling chambers are all shared with multiple other tasks including flight projects like Europa; and, they undergo periodic down-time for maintenance and repairs.

Initial likelihood (1-5): 2
At the time of the proposal, all relevant facilities had capacity far in excess of the EESP project's needs, and they anticipated sparse future usage.

Initial consequence (1-5): 4
Given the aggressive schedule for the Base period, a 1-2 month delay translates into at least one fewer cell development iterations.

Timeframe:
Base, Option I and Option II periods.

Mitigation strategies:
(1) Early and frequent communication with the facility owners to manage priorities and establish firm schedules;
(2) Compressing the time required for each test and exposure (also see Schedule Risk);
(3) Starting the tests and exposures early, e.g. via the 0^{th}-iteration approach;
(4) Searching for and evaluating the suitability of alternative facilities.

Status:
The Base period cell design iterations (0^{th} and 1^{st}) have been completed. JPL now has five projects (including EESP and Europa) all doing cell testing in parallel, leading to increased probability of scheduling conflicts. The X25 and Dynamitron facilities both have multiple-shift capability, although the Dynamitron accelerator has been down for upgrades Jan-May 2017. The NIST facility has been developed as a suitable alternate irradiation facility.

Current likelihood (1-5): 2
Unchanged, after multiple fluctuations.

Current consequence (1-5): 3
Decreased, now that the Base period has been successfully completed. Further reductions are pending completion of the 2^{nd} through 3^{rd} cell iterations, as well as the planned coupon and prototype-panel tests.

Risk #7: Cell Damage

Risk statement:
If test articles suffer from damage due to non-flight-like test artifacts, the quality of data acquired on them may be compromised, jeopardizing our ability to demonstrate the project objectives.

Context:
A recent experience from the Europa Clipper project showed that bare cells are susceptible to breakage from repeated handling during the test and exposure sequence. Also, CIC coupons were found to be susceptible to the delamination of the various silicone bonds, which during test are being subjected to non-flight-like radiation doses and thermal conditions.

Initial likelihood (1-5): 4
IMM4 bare cells and CICs are mechanically similar to the state-of-practice bare cells and CICs that were tested on Europa.

Initial consequence (1-5): 3
Damaged test articles may effectively reduce the development scope, given the fixed schedule and budget.

Timeframe:
Base, Option I and Option II periods.

Mitigation strategies:
(1) using CICs instead of bare cells, which reduces the likelihood of breakage;
(2) eschewing attachment to a substrate for cell performance testing, which eliminates the possibility of cell adhesive delamination and poor thermal contact;
(3) slowing down or eliminating the temperature and pressure ramp rates, and reducing the irradiation flux, which reduces the likelihood of coverglass adhesive delamination;
(4) performing dry run test-irradiate-test sequences on electrical reject (mechanical) samples.

Status:
Mechanical fixtures and test protocols for the above mitigations have been implemented. The 0^{th} iteration irradiation has been successfully completed in the Dynamitron with no damage. Dry run experiments established safe conditions for the NIST facility, and the 1^{st}-iteration irradiation was successfully completed with no damage.

Current likelihood (1-5): 2
Reduced, thanks to multiple successful irradiation rounds.

Current consequence (1-5): 3
Unchanged.

Risk #8: Screening Yield

Risk statement:
If the anticipated LIRT screening yield is not reached upon the conclusion of the 3-period EESP project, this technology's cost to future flight programs may be higher than currently expected.

Context:
The EESP project does not have cost targets for the technology to be developed. Due to limited resources, we had to focus first on meeting the aggressive performance targets; however, reaching high LIRT yields (>90%) does in fact constitute a stretch goal for the project, since it would translate directly into cell-build cost reductions for qualification and flight.

Initial likelihood (1-5): 4
LIRT screening yield is not currently a high-priority goal.

Initial consequence (1-5): 2
Even with yields comparable to the state-of-practice (<40%), the proposed technology would still provide significant cost savings to a flight mission.

Timeframe:
After Option II (flight infusion).

Mitigation strategies:
(1) Obtaining preliminary yield information from the early cell development iterations;
(2) Working on yield optimization, if the performance development effort requires fewer resources than originally planned.

Status:
Based on the 0^{th} and 1^{st} iterations (~40 cells), IMM4 screening yields are in fact high. The decision on whether to pursue yield optimization will be made during early Option II, in preparation for the qualification and manufacturability tasks.

Current likelihood (1-5): 3
Reduced, based on promising albeit low-statistics data so far.

Current consequence (1-5): 2
Unchanged.

Risk #9: Development Cost

Risk statement:
If the cell or array development are significantly more difficult than expected, the cost of the as-planned development may exceed the task's budget.

Context:
Other (e.g., technical or schedule) risks all carry implicit cost impacts, should they come to pass.

Initial likelihood (1-5): 3
This is the likelihood averaged over all other identified risks.

Initial consequence (1-5): 2
Some budget flexibility exists, especially during the Option periods.

Timeframe:
Base, Option I and Option II periods.

Mitigation strategies:
(1) Implementation of judicious risk tracking and management strategy;
(2) Early consideration of possible low-impact scope reductions, to be used as cost margin if needed.

Status:
The risk list has been created and is being maintained. The Base period work has been completed on budget.

Current likelihood (1-5): 3
Unchanged. Reductions in likelihood are pending the completion of the Option I milestones.

Current consequence (1-5): 2
Unchanged. Impact reductions are pending an evaluation of scope flexibility.

Risk #10: Flight Infusion

Risk statement:
If a convincing case is not made for the new technology's viability and readiness, proposal and flight systems teams will delay or prevent its infusion.

Context:
Upon successful completion of the EESP development project (Base through Option II), the array system would be at TRL5+, ready for infusion as a high-performance power source for missions to the Jupiter orbit and beyond. By that point, we will have completed all the array analyses, coupon and panel prototype testing, and cell qualification for the relevant EESP environment.

Initial likelihood (1-5): 3
At the time of the proposal, the IMM4 component had low TRL for the EESP environment, and only limited flight heritage for 1AU.

Initial consequence (1-5): 4
Development success is moot in the absence of infusion.

Timeframe:
After the Option II period.

Mitigation strategies:
(1) Using IMM4 as a power source for an Earth-orbit flight, i.e. 1AU TRL9 for the cell;
(2) Performing in-flight technology demonstrations on IMM4 at 5AU, i.e. LILT TRL7 for the cell;
(3) Demonstrating MegaFlex performance in Earth orbit, i.e. 1AU TRL7-9 for the structure.

Status:
The Surrey OTB satellite, launching on the maiden flight of Falcon 9 Heavy in 2017, will be partially powered by IMM4 cells. Also, the Europa Clipper spacecraft, bound for the Jupiter system and launching in the 2020's, plans to include JPL's EESP IMM4 CICs with in-situ characterization, as a technology demonstration.

Current likelihood (1-5): 2
Reduced, thanks to significant cell-level TRL advancement during the Base period; we will retire this risk upon the successful completion of the above mitigation strategies.

Current consequence (1-5): 4
Unchanged.

Recommendations

As demonstrated by the results described in this report, the work proposed for the Base period has been successfully completed. Downselects have been effected for the cell and array architectures, and a particular array-structure technology has been chosen. In particular, meeting the LILT cell efficiency targets at both BOL and EOL is a significant achievement. Also, our analysis indicates that the proposed system concept will meet the array-level goals. We therefore recommend that the task should continue with the Option I and II development activities, as proposed.

During the Option I period, we plan to continue the cell development at JPL and SolAero, by completing the 2nd and 3rd design iterations, which will increase the cell-level performance margin and reduce the risk for meeting the system-level array requirements. At the end of the Option I period, the LILT/Rad-optimized cell design will be frozen. During the Option II period, cell work will focus on qualification, manufacturability and integration.

For the array structure, we propose for Orbital ATK to provide MegaFlex substrates for the coupon and panel prototype hardware, detailed inputs for the system models, as well as thermal cycling and mechanical testing at the coupon and panel level. We estimate that the majority of the array-structure work will be targeted at verifying the integration with the IMM4 cell, and at validating the overall array-level performance through test and analysis.

A coupon representative of the array technology will be built and tested during the Option I period. We plan for Orbital ATK to build the substrate, SolAero to design the layout, fabricate the cells and integrate them into the coupon, and JPL to perform the majority of validation testing. The coupon performance will be evaluated at 5AU via LAPSS and at LILT in the X25 laboratory, both before and after irradiation up to a total dose of 4e15 1MeV e/cm^2, as well as after thermal cycling to operating and non-operating temperature extremes. Finally, the array's

ability to operate in the 100-300V range in the presence of plasma exhaust fields will be validated in JPL's high-voltage facility.

A scalable prototype panel representative of the array technology will be built and tested during the Option II period. The plan is for Orbital ATK to build the substrate; for SolAero to design the layout, fabricate the cells, integrate them into the panel, and perform LAPSS (large-area pulsed solar simulator) testing; then, for Orbital ATK to integrate the panel into the array system. The panel performance will be evaluated at 1AU and LIRT, both before and after thermal cycling to operating and non-operating temperature extremes, and after simulating the launch environment via acoustic testing.